Research Department

Technical Report No. 62

Atmospheric effective angular momentum functions for 1986-1987

by

G Sakellarides

February 1989

Abstract

Time series of wind and surface pressure for 1986-87 have been used to evaluate Atmospheric Effective Angular Momentum (called hereafter AEAM) functions. Also the implied polar motion of the solid Earth has been calculated as well as the length-of-day using initialized analyses and 3, 5 and 10 day forecasts, from the ECMWF archives.

It is found that both the variations of the AEAM functions as computed from the initialized analyses and the (3, 5 and 10 day) forecasts follow the familiar annual pattern. An analysis of wind and pressure terms of the global equatorial components shows that the largest error arises from the Southern Hemispheric wind contributions. Globally, the wind terms of the equatorial components on average compensate the yearly variations induced by the pressure terms. A comparison of analysed AEAM functions with the prognostic ones enables us to detect model systematic errors, for both axial and equatorial AEAM functions. Looking at the radii of circles traced out by the implied movement of the rotation pole and forced by wind terms of the equatorial components, we found that for 1986 in the Northern Hemisphere the prognostic radius is systematically smaller than that of the initialized analyses, showing that there is not sufficient torque to move the rotation pole to the right position. The model's torque has been increased for 1987 but from the comparison of the radius it can be seen that the torque is slightly higher than the optimum one. In contrast to the Northern Hemisphere there is too much torque in the Southern Hemisphere.

A study of axial AEAM functions in comparison with length-of-day variations reveals that there is an exchange of angular momentum between Earth and atmosphere. A systematic error in the prognostic axial AEAM functions has been found in the Northern Hemisphere since the introduction of the parametrization of gravity-wave drag, suggesting that either the gravity-wave drag is higher than the optimum one, or its introduction has revealed the presence of a compensating error.

CONTENTS

1. INTRODUCTION

Tiny fluctuations in the length of the day and slight movements of the earth's pole of rotation (called polar motion or 'wobble') have been observed since the clocks and the positional astronomy have become more accurate. The fluctuations in the length of the day can be measured by the time intervals between successive passes of a given start across a meridian, while the wobble can be measured by variations in astronomical latitude at a given station.

The length of day exhibits variations of a few milliseconds on timescales from days to years. The rotation pole performs a circular motion with a variable radius of a few metres with a period of about 14 months. Reviews of the variation in the earth's rotation (magnitude and direction) have been given by Munk and MacDonald (1960), and Lambeck (1980).

This paper is concerned with the contribution of the atmosphere to the variable rotation of the solid earth. The magnitude of the atmospheric angular momentum is about 10^{-6} of that of the whole earth, and the fluctations are related to the changes in the strength of the zonal circulation and in the surface pressure distribution. All the components of the atmospheric angular momentum as mentioned before exhibit variations of time scales from a few days to years, and these are related to the changes in the distribution of mass in the atmosphere and in the wind pattern.

In studying the effects of the atmosphere on the rotation of the earth, the forcing functions (called excitation functions) containing all possible effects on the motion of the earth should be evaluated. This can be done by two approaches. In the torque approach, due to the presence and motion of the atmosphere, torques are exerted on the earth's surface and these torques are related to the earth's rate of change of angular momentum. In the angular momentum approach, the rate of change of the earth's angular momentum is considered to be equal and opposite to the rate of change of the atmosphere's angular momentum. The equivalence of these approaches has been described by Munk and MacDonald (1960) and Lambeck (1980). The excitation functions, however, are complex and cannot be evaluated from routine meteorological data, since stresses cannot be estimated accurately from these data. Therefore, Barnes et al. (1983) proposed a new treatment of the excitation functions, by introducing simpler, undifferentiated forcing functions, named Atmospheric Effective Angular Momentum functions which can be evaluated from routine meteorological data.

In this study such AEAM functions have been calculated for ECMWF analyses and forecasts. The separate contributions from the Northern and Southern Hemispheres have been evaluated for 1986 and 1987. The primary purpose of this paper is to give more insight into the fluctuations of the AEAM functions of the analysis and forecast and to find (systematic) errors in the ECMWF global model. A detailed discussion of the adiabatic formulation of the model can be found in Simmons et al. (1988), of the parametrizations in Tiedtke et al. (1979), Miller and Palmer (1986), and Tiedtke et al. (1988) and the analysis scheme in Shaw et al. (1987).

The outline of this paper is as follows. In section 2 the dynamics of the earth's rotation leading to the formulation of AEAM functions are presented. In section 3 the results are discussed and finally in section 4 the conclusions are presented.

2. DYNAMICS OF THE EARTH'S ROTATION

2.1 Fundamental equations

The Eulerian equations of motion (earth and atmosphere) in a coordinate system x_i (i=1,2,3), coinciding for the moment with the principal axes of the solid earth and rotating with angular velocity ω_i, about its centre of mass, are:

$$\frac{dH_i}{dt} + \varepsilon_{ijk}\,\omega_j\,H_k = L_i \qquad (2.1)$$

where:

$L_i = \vec{r}_i \times \vec{F}_i$ are the components of externally applied torque,

ε_{ijk} is the alternating tensor, zero if any two subscripts are equal, +1 if subscripts are in even order, -1 if they are in odd order,

H_i is the absolute angular momentum, which is given by:

$$H_i = I_{ij}(t)\,\omega_j + h_i \qquad (2.2)$$

where $I_{ij} = \int_V \rho(x_k x_k \delta_{ij} - x_i x_j)\,dV$ is the variable inertia tensor for matter contained in the volume V,

ρ is the density,

δ_{ij} is the Kronecker delta, and finally

$h_i = \int_V \rho\,\varepsilon_{ijk}\,x_j\,u_k\,dV$ is the relative momentum due to motion u_i relative to the x_i - system.

Equation (2.1) describes the response of the whole earth to an externally applied torque. The terms L_i, H_i and I_{ij} include the contribution of the earth and the atmosphere. Substitution of (2.2) into (2.1) leads to

$$\frac{d}{dt}(I_{ij}\,\omega_j + h_i) + \varepsilon_{ijk}\,\omega_j\,(I_{kl}\,\omega_l + h_k) = L_i \qquad (2.3)$$

This equation was derived by Liouville in 1858 (Routh, 1905).

2.2 Solutions to the Liouville equations

The Liouville equations can be simplified by a perturbation scheme (Munk and MacDonald (1960)), assuming the departure from rigidity to be small.

Defining:

$$I_{ij} = \begin{pmatrix} A + a_{11} & a_{12} & a_{13} \\ a_{12} & A + a_{22} & a_{23} \\ a_{13} & a_{23} & C + a_{33} \end{pmatrix} \tag{2.4}$$

where a_{ij} are the moments and products of perturbations in the inertia tensor, A is the equatorial moment of inertia, and $C=7.04 \times 10^{+37}$ kg m^2 is the polar moment of inertia of the solid earth. The relation between A and C is given by (C-A)/C = 0.00333. Since the rotation of the earth departs only slightly from steady rotation about the polar axis, the angular velocity vector can be written as:

$$(\omega_1, \omega_2, \omega_3) = (m_1, m_2, 1 + m_3)\, \Omega \tag{2.5}$$

where Ω is the mean angular velocity of the earth, and m_1, m_2 and m_3 are the direction cosines of the rotation axes relative to the reference axes. Because the quantities a_{ij}/C, m_i and $h_i/(\Omega C)$ are small, and ignoring products and squares of them, the Liouville equations (2.3) can be reduced to:

$$\frac{\dot{m}_1}{\sigma_r} + m_2 = Y_2$$

$$\frac{\dot{m}_2}{\sigma_r} - m_1 = -Y_1 \tag{2.6}$$

$$\dot{m}_3 = \dot{Y}_3$$

where:

$$\sigma_r = \frac{C - A}{A}\ \Omega$$

is the Eulerian or rotation frequency. The corresponding observed Chandler's period is 14 months.

The Y_1, Y_2 and Y_3 are defined by the following equations:

$$\Omega^2 (C-A) Y_1 = \Omega^2 a_{13} + \Omega \dot{a}_{23} + \Omega h_1 + \dot{h}_2 - L_2$$

$$\Omega^2 (C-A) Y_2 = \Omega^2 a_{23} - \Omega \dot{a}_{13} + \Omega h_2 - \dot{h}_1 + L_1 \qquad (2.7)$$

$$\Omega^2 C Y_3 = \Omega^2 a_{33} - \Omega h_3 + \Omega \int_0^t L_3 \, dt$$

where the (˙) stands for $\frac{d}{dt}$.

The dimensionless forcing term Y_i is known as the 'excitation function'. By defining m and ψ in the complex plane as: $m=m_1+im_2$, $\psi=Y_1 + iY_2$, the equations (2.6) can be written

$$\dot{m} - i \sigma_r m = -i\sigma_r \psi$$

$$\dot{m}_3 = \dot{Y}_3 \qquad (2.8)$$

If at t=0 m=m(0) then the solution of (2.8) is given by:

$$m(t) = e^{i\sigma_r t} (m(0) - i \sigma_r \int_0^t \psi(\tau) e^{-i\sigma_r \tau} d\tau) \qquad (2.9)$$

$$m_3 = Y_3 + c \qquad (2.10)$$

In the absence of external forces equation (2.10) expresses the conservation of angular momentum about the x_3-axis, that is

$$\Omega C (1+m_3) + \Omega a_{33} + h_3 = \text{constant}$$

The length of the day Λ can be evaluated from

$$\Lambda = \frac{2\pi}{\omega_3} \qquad (2.11)$$

where $\omega_3 = (1+m_3)\,\Omega$ and $m_3 = Y_3+c$.

If Y_3 can be evaluated from meteorological data, then the length-of-day can be estimated from (2.11).

In order to investigate the excitation of polar motion (wobble) from equation (2.9), the excitation function $\psi=Y_1 + iY_2$ should be evaluated from meteorological data. In case of a free wobble of a rigid earth $\psi=0$. The solution to equation (2.9) is $m(t) = \exp(i\sigma_r t)\, m(0)$ with a ten month period ($2\pi/\sigma_r$). The effect of the earth's deformation is to increase this period by about 40 percent, while Chandler (1891, 1892) discovered a 14 month period. The excitation function ψ is related to the equatorial components of the total torque between the earth and the atmosphere. In the absence of external torques ψ is related to the equatorial components of the rate of change of the atmosphere's angular momentum, which is equal to the total torque acting on the atmosphere. In the absence of external forces this is the total frictional and pressure torque acting at the surface of the earth.

2.3 Atmospheric angular momentum functions

Since the excitation functions are complicated and stresses cannot be evaluated with any precision from routine meteorological data, Barnes et al. (1983) proposed a new treatment of the wobble excitation problem. They introduced the following undifferentiated forcing function:

$$\tilde{X} = \tilde{X}_1 + i\,\tilde{X}_2 = \frac{\Omega\, a + h}{\Omega\,(C-A)} \tag{2.12}$$

where $a = a_{13} + ia_{23}$ and $h = h_1 + ih_2$.

Therefore equation (2.8) can be written as

$$m + \frac{i}{\sigma_r}\,\dot{m} = \tilde{X} - \frac{i}{\Omega}\,\dot{\tilde{X}} \tag{2.13}$$

Integrating eq. (2.13) and transforming to spherical polar coordinates results in:

$$\Omega(C-A)\tilde{X}_1 = -\int_V \rho r\,(\Omega r \sin\varphi\cos\varphi\cos\lambda + u\sin\varphi\cos\lambda - v\sin\lambda)\,dV$$

$$\Omega(C-A)\tilde{X}_2 = -\int_V \rho r\,(\Omega r \sin\varphi\cos\varphi\sin\lambda + u\sin\varphi\sin\lambda + v\cos\lambda)\,dV \tag{2.15}$$

$$\tilde{X}_3 = -Y_3 \tag{2.16}$$

The functions $\tilde{X}_1$ and $\tilde{X}_2$ are called the equatorial angular momentum functions of the atmosphere. The component $\tilde{X}_3 = -Y_3$ is called the axial angular momentum function of the atmosphere. The angular momentum functions of the atmosphere are dimensionless. The non-dimensionalizing factor for $\tilde{X}_3$ $(1/\Omega C)$ is different in magnitude from $1/\Omega(C-A)$ used for $\tilde{X}_1, \tilde{X}_2$. The vector $(\tilde{X}_1, \tilde{X}_2, \tilde{X}_3)$ is therefore not parallel to the atmospheric angular momentum vector.

All components of the angular momentum functions consist of two terms. In the first term the wind is involved, and this is called the wind or motion term, while in the second term the surface pressure is involved and this is called the matter or pressure term. The new functions defined by Barnes et al. (1983) are simpler undifferentiated forcing functions, and they can be evaluated from meteorological data. Following Barnes et al. (1983), assuming that the atmosphere can be treated as a thin spherical annulus of radius R, and that the vertical pressure gradient is given by the hydrostatic relation, the following final form of the atmospheric angular momentum functions is obtained.

$$\tilde{X} = \tilde{X}^p + \tilde{X}^w = -\frac{R^4}{g(C-A)} \iint P_s \sin\varphi \cos^2\varphi \, e^{i\lambda} \, d\lambda \, d\varphi$$

$$-\frac{R^3}{g\Omega(C-A)} \iiint (u\sin\varphi + iv) \cos\varphi \, e^{i\lambda} \, d\lambda \, d\varphi \, dp \qquad (2.17)$$

$$\tilde{X}_3 = \tilde{X}_3^p + \tilde{X}_3^w = \frac{R^4}{gC} \iint P_s \cos^3\varphi \, d\lambda \, d\varphi + \frac{R^3}{gC\Omega} \iiint u\cos^2\varphi \, d\lambda \, d\varphi \, dp$$

Where:

$$\iint (\;) \, d\lambda \, d\varphi = \int_{-\frac{\pi}{2}}^{\frac{\pi}{2}} \int_0^{2\pi} (\;) \, d\lambda \, d\varphi \text{ and}$$

$$\iiint (\;) \, d\lambda \, d\varphi \, dp = \int_0^{P_s} \int_{-\frac{\pi}{2}}^{\frac{\pi}{2}} \int_0^{2\pi} (\;) \, d\lambda \, d\varphi \, dp$$

2.4 Love number corrections and atmospheric effective angular momentum functions

So far the equations have been derived by assuming that the solid earth is perfectly rigid. For a deformable earth the equations are still valid, but the deformation of the earth under prescribed

stresses should be considered. So it is necessary to consider changes in the inertia tensor $I_{ij}^{(e)}$ of the solid earth which may arise from tidal, centrifugal or frictional forces. The surface stresses can be due to atmospheric pressure or wind drag.

The torque on the earth leads to rotational and surface loading deformation and their effects are allowed by using Love numbers (Munk and Mcdonald, 1960; Lambeck, 1980).

Taking into account the Love numbers and both rotational and surface loading deformation the equatorial functions and the wobble are defined (Barnes et al., 1983) by:

$$X = 1.00\,\tilde{X}^{p} + 1.43\,\tilde{X}^{w} \tag{2.18}$$

$$m(t) = e^{i\sigma_o t}\left[m(0) - i\sigma_o\left(1+\frac{\sigma_o}{\Omega}\right)\int_0^t X(\tau)\, e^{-\sigma_o \tau}\, d\tau\right] - \frac{\sigma_o}{\Omega}\left[X(t) - e^{i\sigma_o t} X(0)\right] \tag{2.19}$$

where: $\sigma_o = \sigma_r (k_o - k_2)/k_o$, $k_2 = 0.285$ from the observations of the body tide

and: $(1+2k_2(C-A)/k_o C) = 1.002$,

and: $X_3 = (0.70\,\Omega\, a_{33} + h_3)/\Omega C$ (2.20)

The equatorial (X_1, X_2) and the axial (X_3) components are called the equatorial and axial atmospheric effective angular momentum (AEAM) functions of the atmosphere. The complete form, which is suitable for evaluation of AEAM functions is given by:

$$X_1 = X_1^p + X_1^w = \frac{-1.00\,R^4}{(C-A)\,g}\int_{-\frac{\pi}{2}}^{\frac{\pi}{2}}\int_0^{2\pi} p_s \sin\varphi \cos^2\varphi \cos\lambda\, d\lambda\, d\varphi -$$

$$\frac{1.43\,R^3}{\Omega(C-A)\,g}\int_0^{p_s}\int_{-\frac{\pi}{2}}^{\frac{\pi}{2}}\int_0^{2\pi} (u\sin\varphi\cos\varphi\cos\lambda - u\cos\varphi\sin\lambda)\, d\lambda\, d\varphi\, dp$$

$$X_2 = X_2^p + X_2^w = \frac{-1.00\ R^4}{(C-A)g} \int_{-\frac{\pi}{2}}^{\frac{\pi}{2}} \int_0^{2\pi} p_s \sin\varphi \cos^2\varphi \sin\lambda d\lambda d\varphi -$$

$$\frac{1.43\ R^3}{\Omega(C-A)\ g} \int_0^{p_s} \int_{-\frac{\pi}{2}}^{\frac{\pi}{2}} \int_0^{2\pi} (u\sin\varphi \cos\varphi \sin\lambda + u\cos\varphi \cos\lambda) d\lambda d\varphi d$$

$$X_3 = X_3^p + X_3^w = \frac{0.70\ R^4}{Cg} \int_{-\frac{\pi}{2}}^{\frac{\pi}{2}} \int_0^{2\pi} p_s \cos^3\varphi d\lambda d\varphi + \frac{R^3}{C\Omega g} \int_0^{p_s} \int_{-\frac{\pi}{2}}^{\frac{\pi}{2}} \int_0^{2\pi} u\cos^2\varphi d\lambda d\varphi dp$$

In order to evaluate the AEAM functions for the ECMWF model, the expressions for X_1, X_2 and X_3 have been formulated as follows.

$$X_1 = (-1.00\ R^4)/((C-A)g) \int_{-1}^{1} \int_0^{2\pi} p_s \mu \sqrt{1-\mu^2} \cos\lambda d\lambda d\mu -$$

$$(1.43R^3)/(\Omega(C-A)g) \int_0^1 \int_{-1}^{1} \int_0^{2\pi} ((u\mu\cos\lambda - v\sin\lambda)/\sqrt{1-\mu^2})\, d\lambda d\mu \frac{\partial p}{\partial \eta} d\eta \qquad (2.21)$$

$$X_2 = (-1.00\ R^4)/((C-A)g) \int_{-1}^{1} \int_0^{2\pi} p_s \mu \sqrt{1-\mu^2} \sin\lambda d\lambda d\mu -$$

$$(1.43\ R^3)/(\Omega(C-A)g) \int_0^1 \int_{-1}^{1} \int_0^{2\pi} ((u\mu\sin\lambda + v\cos\lambda)/\sqrt{1-\mu^2}) d\lambda d\mu \frac{\partial p}{\partial \eta} d\eta \qquad (2.22)$$

$$X_3 = (0.70\ R^4)/(Cg) \int_{-1}^{1} \int_0^{2\pi} p_s (1-\mu^2) d\lambda d\mu + (R^3/C\Omega g) \int_0^1 \int_{-1}^{1} \int_0^{2\pi} u d\lambda d\mu \frac{\partial p}{\partial \eta} d\eta \qquad (2.23)$$

where $\sin\varphi = \mu$ and $u\cos\varphi, v\cos\varphi$ have been replaced by u and v respectively.

The final form which is suitable for calculation of AEAM functions for values defined at Gaussian latitudes and hybrid levels is given by:

$$X_1 = \sum_{i=1}^{NGL} w_i (2\pi/NLON) \sum_{j=1}^{NLON} \varepsilon_{ij}^{1p} + \sum_{i=1}^{NGL} w_i (2\pi/NLON) \sum_{j=1}^{NLON} \sum_{k=1}^{NLEV} \varepsilon_{ijk}^{1w} \Delta p_{ijk} \quad (2.24)$$

$$X_2 = \sum_{i=1}^{NGL} w_i (2\pi/NLON) \sum_{j=1}^{NLON} \varepsilon_{ij}^{2p} + \sum_{i=1}^{NGL} w_i (2\pi/NLON) \sum_{j=1}^{NLON} \sum_{k=1}^{NLEV} \varepsilon_{ijk}^{2w} \Delta p_{ijk} \quad (2.25)$$

$$X_3 = \sum_{i=1}^{NGL} w_i (2\pi/NLON) \sum_{j=1}^{NLON} \varepsilon_{ij}^{3p} + \sum_{i=1}^{NGL} w_i (2\pi/NLON) \sum_{j=1}^{NLON} \sum_{k=1}^{NLEV} \varepsilon_{ijk}^{3w} \Delta p_{ijk} \quad (2.26)$$

where:

W_i are the Gaussian integration weights,

NGL is the number of Gaussian latitudes,

NLON is the number of points along a Gaussian latitude,

NLEV is the number of vertical levels

$\varepsilon_{ij}^{1p} = -((1.00\, R^4)/((C-A)g))\, p_s\, \mu\sqrt{1-\mu^2}\, \cos\lambda$

$\varepsilon_{ijk}^{1w} = -((1.43\, R^3)/(\Omega(C-A)g\sqrt{1-\mu^2}))\, (u\mu\cos\lambda - v\sin\lambda)$

$\varepsilon_{ij}^{2p} = -((1.00\, R^4)/((C-A)g)\, p_s\, \mu\sqrt{1-\mu^2}\, \sin\lambda$

$\varepsilon_{ijk}^{2w} = -((1.43\, R^3)/(\Omega(C-A)g\sqrt{1-\mu^2}))(u\mu\sin\lambda + v\cos\lambda)$

$\varepsilon_{ij}^{3p} = ((0.70\, R^4)/(Cg))(1-\mu^2)p_s$

$\varepsilon_{ijk}^{3w} = (R^3/(C\Omega g))\, u$ and

R is the radius of the Earth.

3. RESULTS

The equatorial component of the AEAM functions (X_1, X_2) and the axial component (X_3) have been calculated by equations (2.24), (2.25) and (2.26). The contribution from the globe and the Northern and Southern Hemisphere have been calculated for both the wind (X_1^w, X_2^w, X_3^w) and the pressure (X_1^p, X_2^p, X_3^p) terms. In the presentation of the time series the data have been smoothed by an eleven-day running mean which has been chosen arbitrary to cut out the high frequency noisy raw data. In all plots the analysis is presented by a continuous heavy curve and the ten, five and three day forecasts by thin continuous, dotted and dashed curves respectively. The scale factor for each component is shown on the vertical coordinate axes. For comparison with the paper of Barnes et al. (1983) the scale factor for the axial component has been multiplied by $q=C\Omega=5.133568.10^{33}$. For polar movements the units of the ordinate are seconds of arc. One second of arc is $4.848.10^{-6}$ rad, which corresponds to a displacement of about 31m at the earth's surface.

3.1 Equatorial components of atmosphere effective angular momentum functions

The equatorial components of the AEAM functions (X_1, X_2) have been examined separately for the Globe and the Northern and Southern Hemisphere.

3.1.1 Contribution to X_1, X_2 from the Northern Hemisphere

The components X_1, X_2 for this hemisphere for 1986 and 1987 are shown in Fig. 1a,b,c and Fig. 2a,b,c. As in previous studies (for example Barnes et al., 1983) the X_2^p (Fig. 2c) exhibit a marked yearly sinusoidal variation with a period close to that of the Chandler wobble, with rapid variations superimposed. In the yearly variation of X_2^p the main maximum occurs during the Northern Hemispheric summer. The X_2^w term (Fig. 2b) exhibits a similar but opposite variation, with smaller amplitude, having a minimum during the Northern Hemispheric summer. Therefore the X_2^w term (Fig. 2a) compensates the X_2^p term. For both years the terms X_1^p (Fig. 1c) and X_1^w (Fig. 1b) suggest a yearly variation of small amplitude. As for the X_2 term, the variations in X_1^p and X_1^w are of opposite direction. A systematic error in X_1^w and X_1^p terms (Fig. 1b,c) has been found, with a tendency for the model to overestimate X_1^w and X_1^p, mainly during the Northern Hemispheric summer.

3.1.2 Contribution to X_1, X_2 from the Southern Hemisphere

The terms X_1^w (Fig. 3b) and X_1^p (Fig. 3c) exhibit fairly constant values throughout the year. A systematic error is seen in the X_1^w term, with a tendency of the model to overestimate this component during the Southern Hemispheric winter.

The curves of terms X_2^p (Fig. 4c) and X_2^w (Fig. 4b) for the analysis exhibit a fairly level yearly values with more rapid variations superimposed. There is a considerable systematic error in the prognostic X_2^w terms during the Southern Hemispheric winter. The prognostic 3-day X_2^w term (Fig. 4b) has the largest bias compared with the initialized analysis, indicating a "spin-up" problem, which may be related to the known spin-up problem in tropical precipitation (Illari, 1987). An analysis of integrated wind error (figures are not shown) for July 86 and 87, shows that the largest errors are well related to the X_2 wind term errors, indicating that the wind error is mainly responsible for this large biases in X_2 wind term (Fig. 4b).

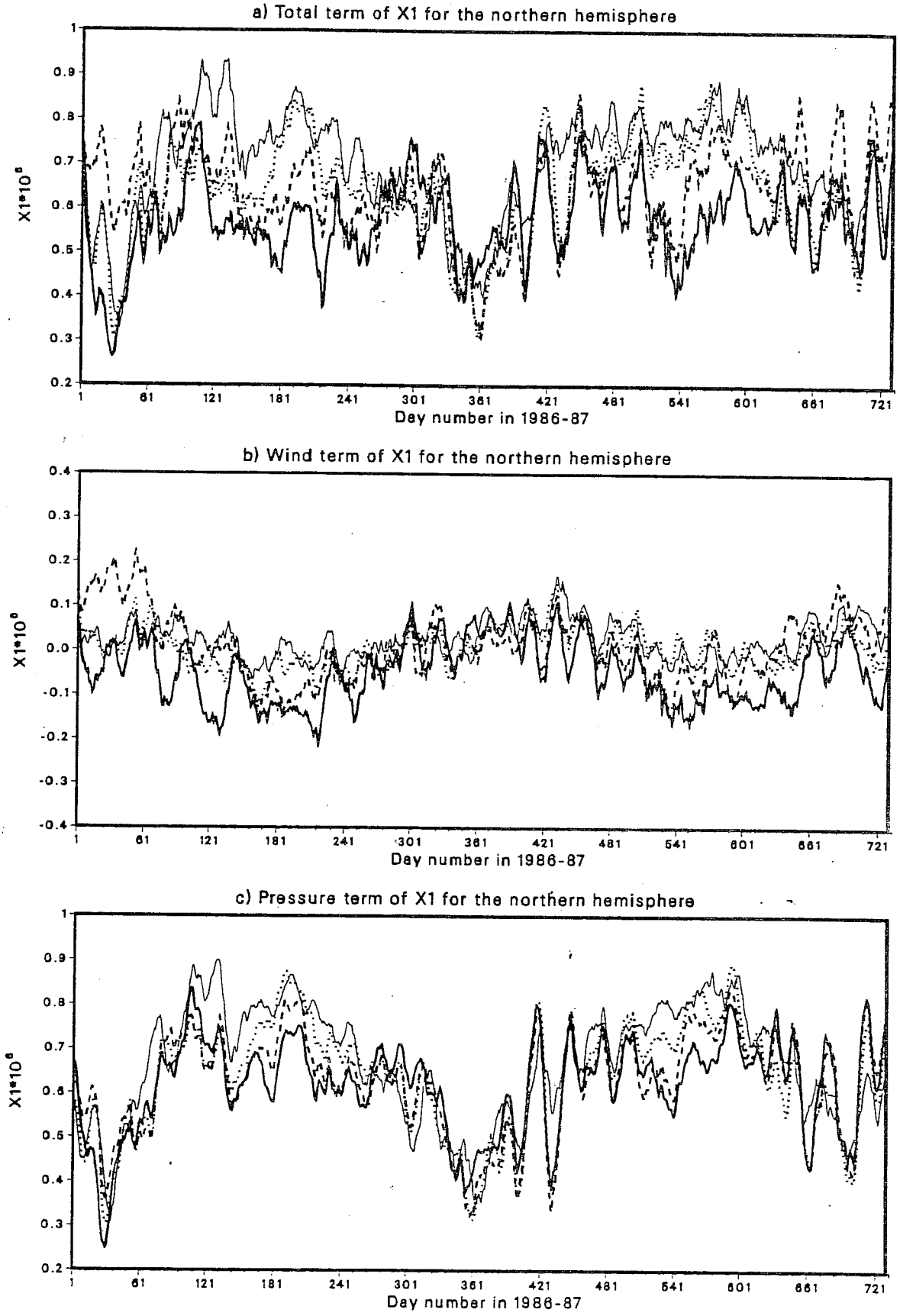

Fig. 1 Equatorial components X_1 of AEAM functions for the Northern Hemisphere for 1986-1987. The analysis is presented by a continuous heavy curve, the ten-day forecast by a thin continuous curve, the five-day forecast by a dotted curve and finally the three-day forecast by a dashed curve. The scale factor is shown on the vertical coordinate axes.

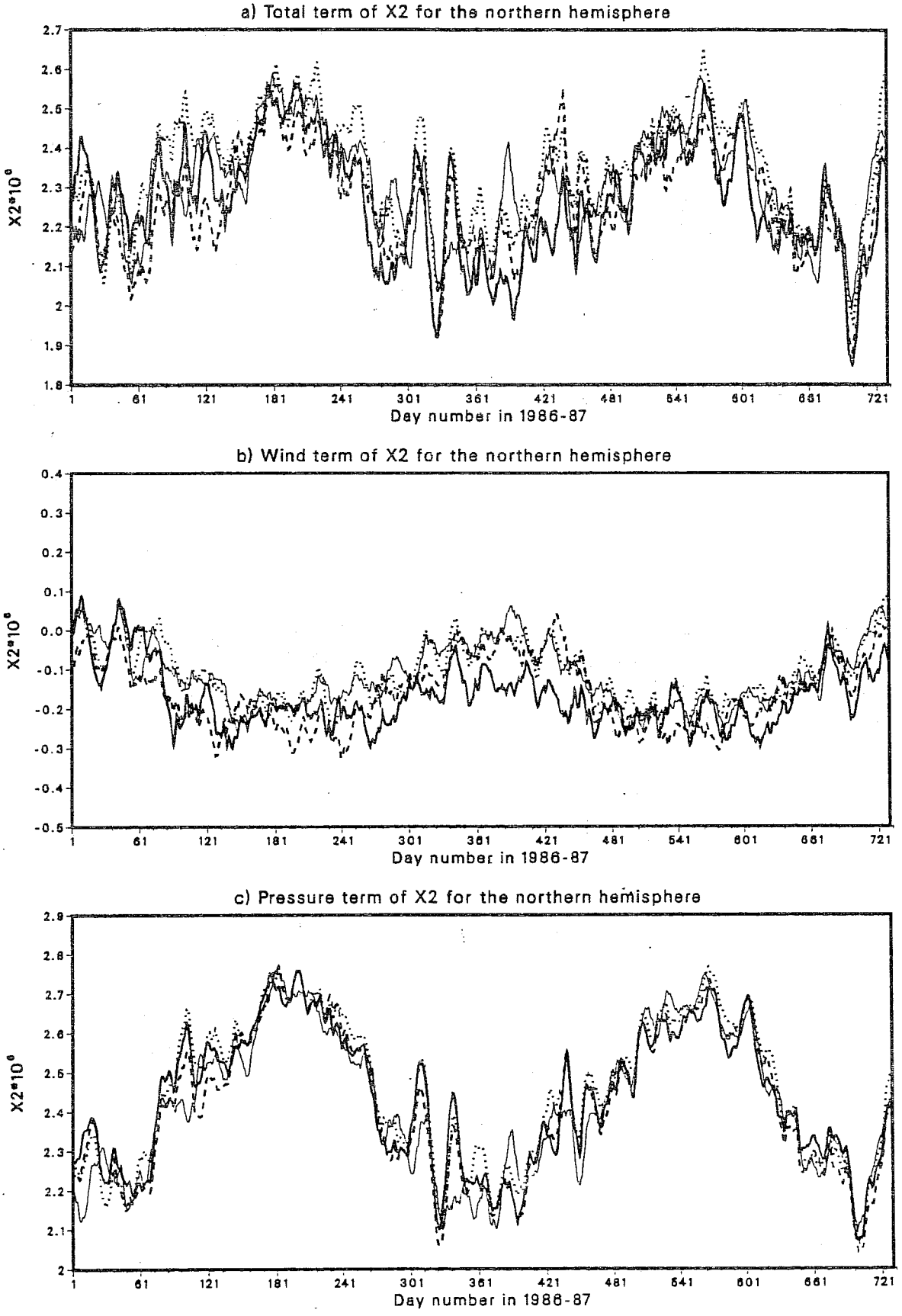

Fig. 2 As in Fig. 1 but for the equatorial components X_2.

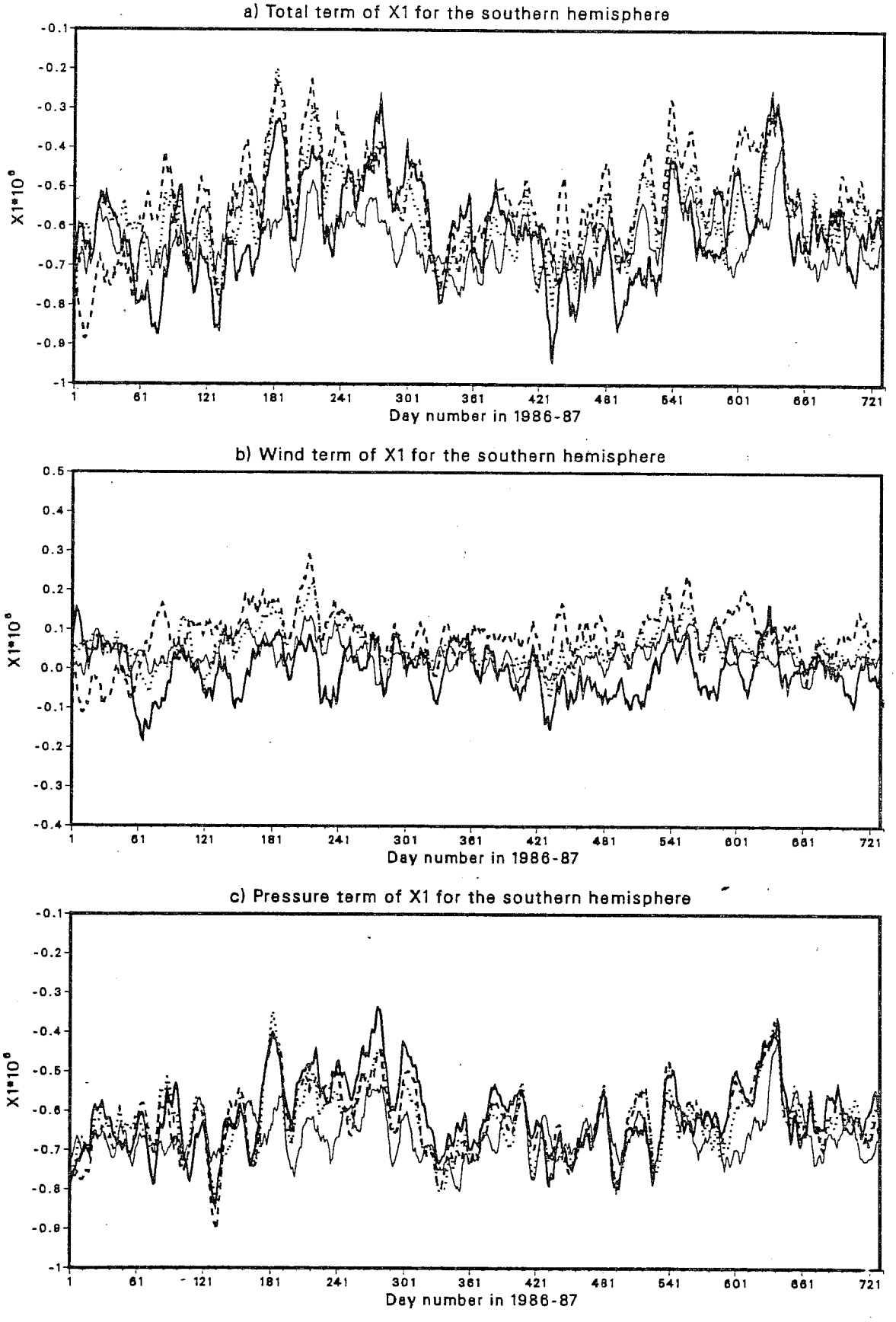

Fig. 3 As in Fig. 1 but for the Southern Hemisphere.

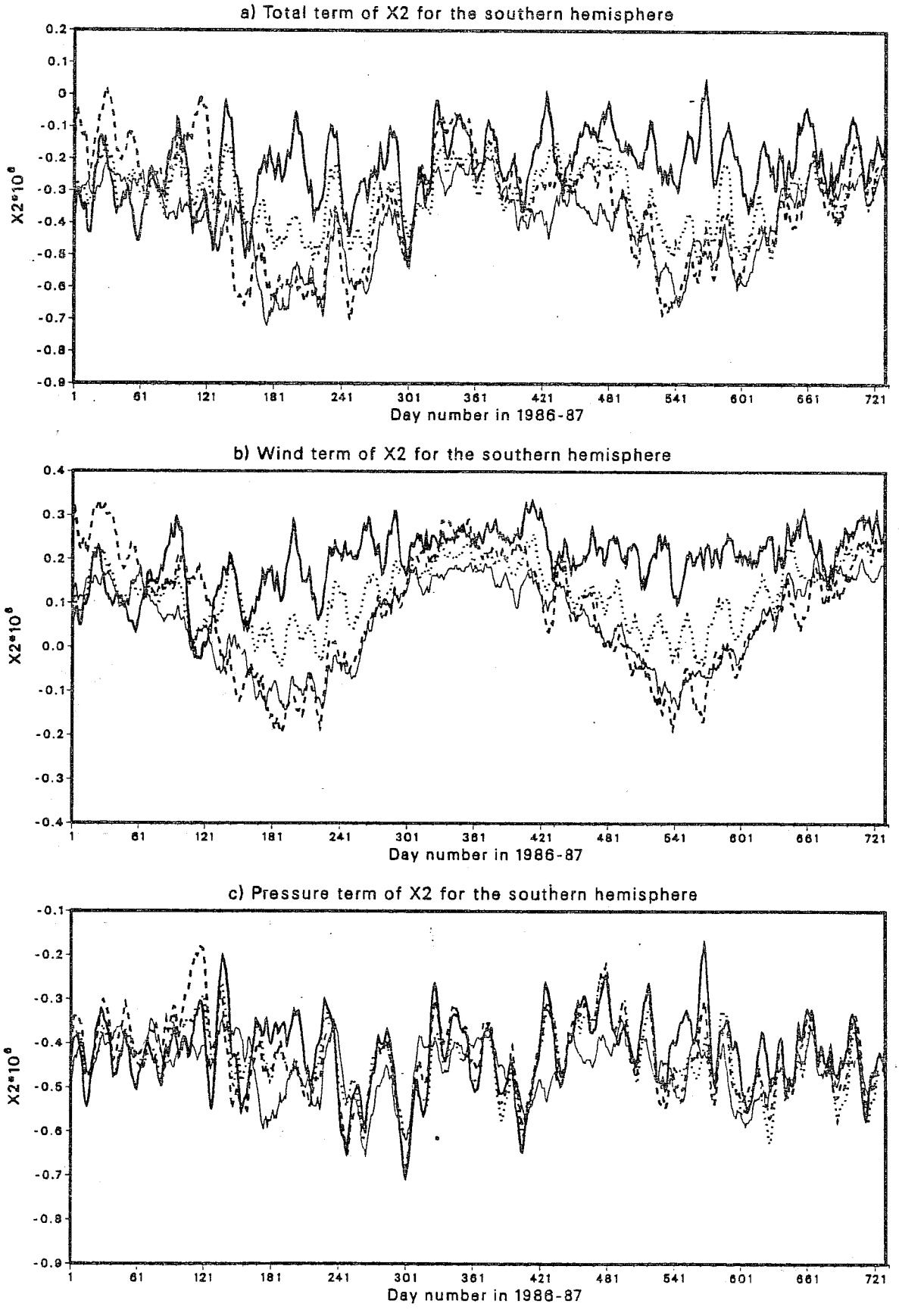

Fig. 4 As in Fig. 2 but for the Southern Hemisphere.

3.1.3 Global contribution to X_1, X_2 terms

For both years the terms X_1^p (Fig. 5c) and X_2^p (Fig. 6c) suggest a sinusoidal variation with a period close to that of the Chandler wobble and with rapid variations superimposed. The amplitude of X_2^p is larger than X_1^p. The terms X_1^w(Fig. 5b) and X_2^w (Fig. 6b) exhibit a similar but opposite yearly variation to X_1^p and X_2^p respectively. Since the wind and pressure terms have on average an opposite sign, the amplitude of the total (X_1, X_2) is smaller than the amplitude of (X_1^p, X_2^p). Generally, in the total component (X_1, X_2) the characteristics of the Northern Hemisphere variations are present. This is due to the fact that the equatorial components of pressure and friction torques are more pronounced in the Northern Hemisphere due to the presence of more orography and land sea contrasts. There are systematic errors in the X_1^w and X_2^w terms, and there is evidence of the spin-up problem in the prognostic 3-day wind term (X_2^w). The model's tendency is to overestimate X_1^w and underestimate X_2^w, mainly during the Northern Hemispheric summer.

3.2 Amplitude and phase error of $X=X_1+iX_2$

The phase error of the forecast $X=X_1+iX_2$ has been defined by:

$$\text{phase error} = \begin{cases} -\cos^{-1}(X_2/|X|)_F - \cos^{-1}(X_2/|X|)_A & \text{for } (X_2)_F > 0,\ (X_2)_A < 0 \\ -\cos^{-1}(X_2/|X|)_F + \cos^{-1}(X_2/|X|)_A & \text{for } (X_2)_F > 0,\ (X_2)_A > 0 \\ \cos^{-1}(X_2/|X|)_F - \cos^{-1}(X_2/|X|)_A & \text{for } (X_2)_F < 0,\ (X_2)_A < 0 \\ \cos^{-1}(X_2/|X|)_F + \cos^{-1}(X_2/|X|)_A & \text{for } (X_2)_F < 0,\ (X_2)_A > 0 \end{cases}$$

where F stands for forecast and A for the analysis. In case of the analysis the phase error is zero. Obviously the phase error is in the interval $[-\pi,+\pi]$.

The amplitude has been defined by:

$$\text{Amplitude of } X = |X| = \sqrt{X_1^2 + X_2^2}$$

3.2.1 Global contribution to $X=X_1+iX_2$

The yearly variations of the amplitude of X (Fig. 7) are dominated by the annual variations of X_2, since X_2 is of higher amplitude. The prognostic amplitude of the pressure term of the 3 and 5 day forecast of X (Fig. 7c) follows the analysis quite reasonably. This term shows a yearly variation with maxima during the Northern Hemispheric summer. In the wind term of the amplitude of X (Fig. 7b)

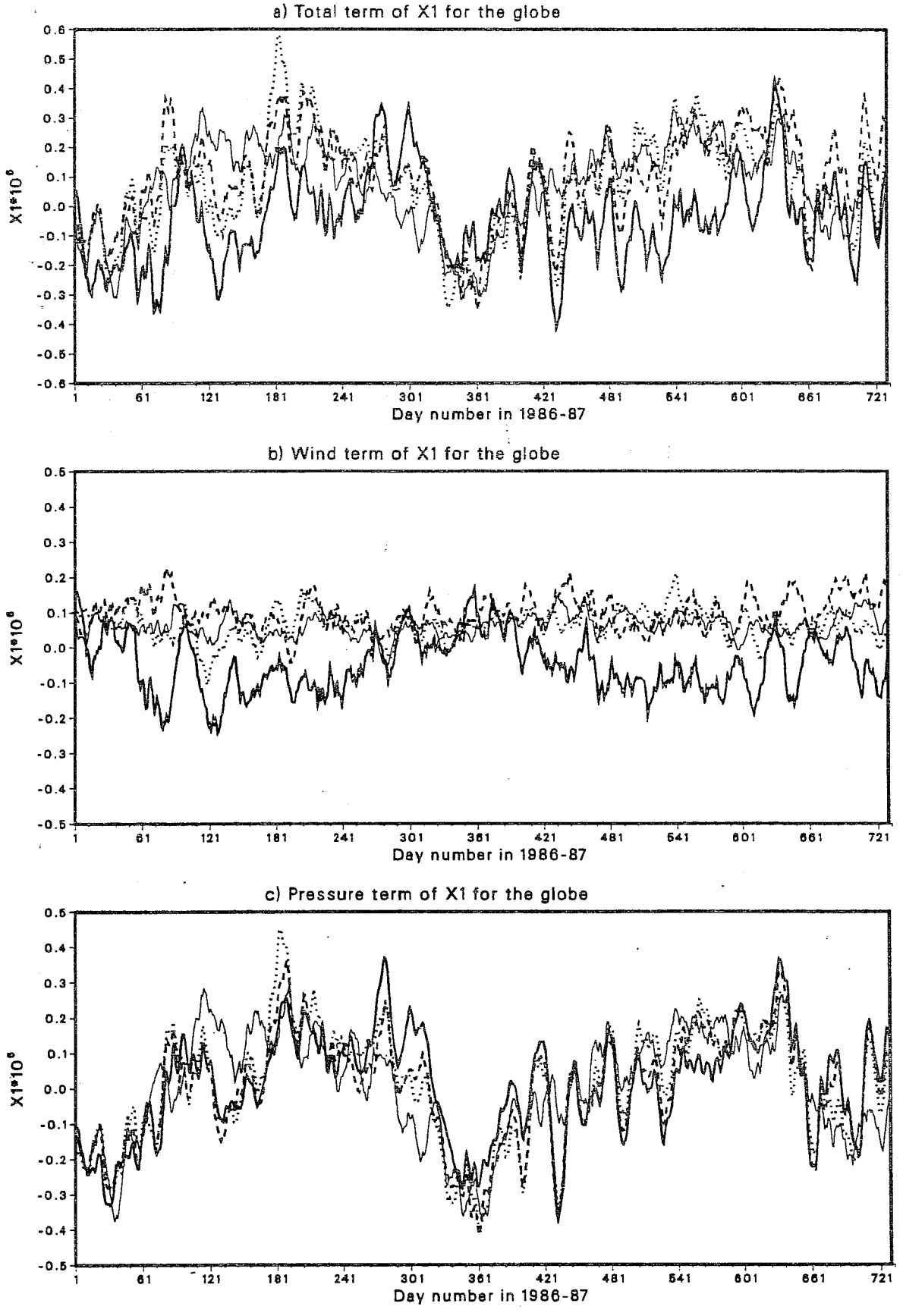

Fig. 5 As in Fig. 1 but for the Globe.

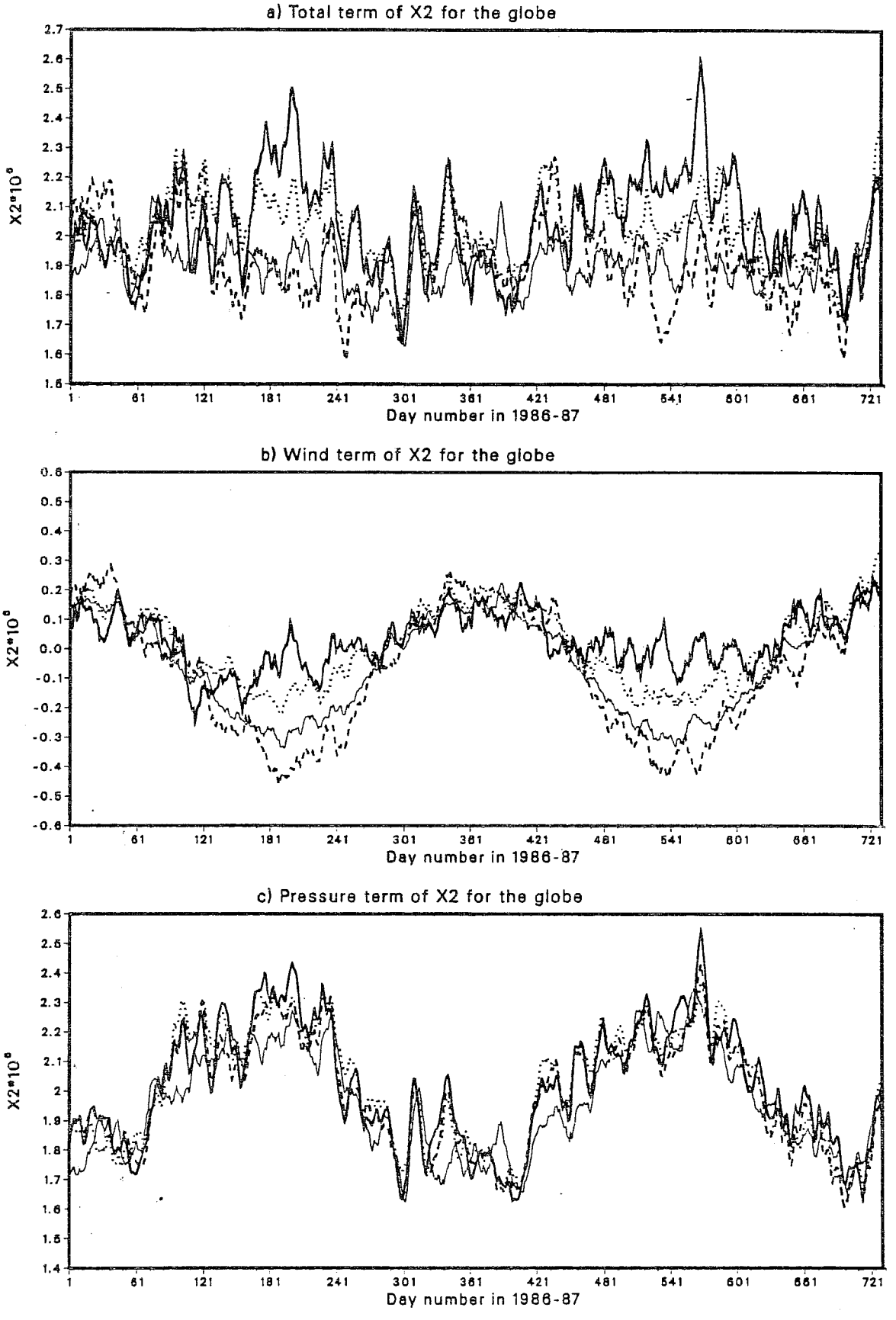

Fig. 6 As in Fig. 5 but for the component X_2.

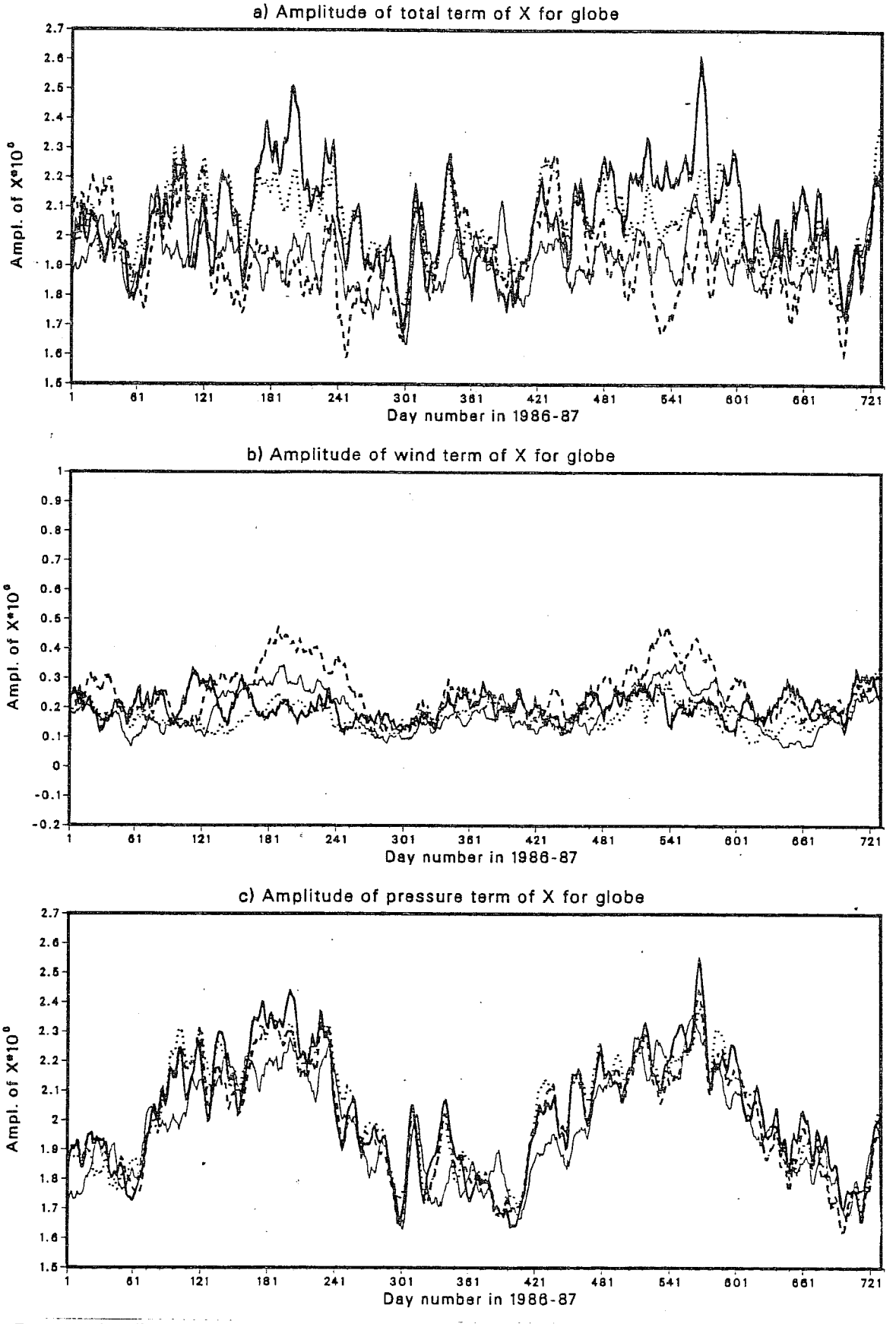

Fig. 7 Amplitude of $X=X_1+iX_2$ for the Globe for 1986-1987. The convention for the type of curves is the same as in Fig. 1.

the large wind term error of X_2 of the Southern Hemisphere is dominant, since the biases of the 3-day forecast are the largest, mainly during the Northern Hemispheric summer. In the total term (Fig. 7a) the prognostic amplitude is systematically smaller than the analysis and mainly during the Northern Hemispheric summer. Large phase errors (Fig. 8) have been found in the wind term (Fig. 8b) in comparison with the pressure (Fig. 8c) and total (Fig. 8a) terms.

3.3 Polar motion (wobble)

The displacement of the pole of rotation around the geographical reference pole, has been calculated according to equation (2.19). Before the discussion of the results, let us consider the first effect of a simple excitation function $\psi(Y_1, Y_2)$ to the wobble equation as defined by Barnes et al. (1983).

$$m + (i/\sigma_0)\dot{m} = \psi \tag{3.1}$$

If $\psi(Y_1, Y_2)$ is constant, then the solution is an anticlockwise motion of the pole of rotation around the excitation pole, with an angular velocity σ_0 and radius of $(m(0)-\psi)$. When ψ is a function of time, the pole of rotation follows a non-circular path. The component (Y_1, Y_2) are related to (X_1, X_2) by the expression

$$Y_1 = X_1 + \dot{X}_2/\Omega$$

$$Y_2 = X_2 - \dot{X}_1/\Omega \tag{3.2}$$

Global components Y_1, Y_2 have been calculated (figures are not shown). The Y_1, Y_2 follow the fluctuations of X_1, X_2 suggesting that the terms $\dot{X}_1/\Omega$ and $\dot{X}_2/\Omega$ are of smaller magnitude. Since $|\dot{m}/\sigma| \sim |m|$ (Barnes et al., 1983) the following relation has been adopted (derived from (2.19)) for calculating initial values of X_1, X_2

$$X_1 \sim m_1 - m_2$$

$$X_2 \sim m_1 + m_2 \tag{3.3}$$

If the initial coordinates (m_1^0, m_2^0) of the pole are known, then from (3.3) the initial values (X_1^0, X_2^0) can be estimated. The initial location of the geographical pole (m_1^0=0.1952, m_2^0=0.178 for 1986 and $m_1^0=9.6510^{-2}$, m_2^0=0.385 for 1987) has been chosen to have the position given by Bureau International de L'Heure (BIH) for the first of January 1986 and 1987 respectively.

The pole displacement calculated by equation (2.19) is strongly dependent on the position of the initial geographical pole. Below, an attempt will be made to investigate the pole movements, bearing

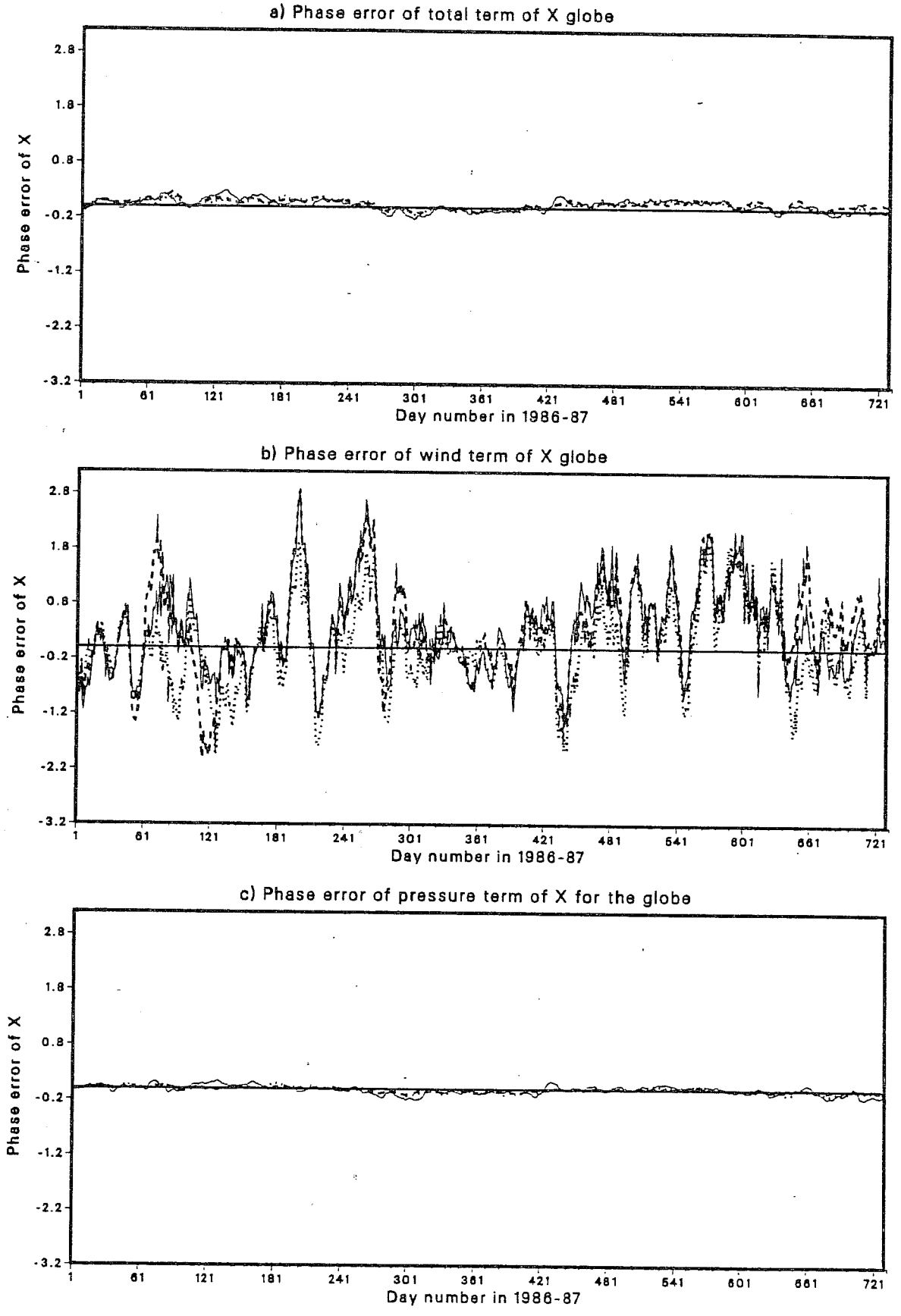

Fig. 8 As in Fig. 7 but for the prognostic phase error, which has been defined in Section 3.2. The phase error of the analysis is zero.

the large wind term error of X_2 of the Southern Hemisphere is dominant, since the biases of the 3-day forecast are the largest, mainly during the Northern Hemispheric summer. In the total term (Fig. 7a) the prognostic amplitude is systematically smaller than the analysis and mainly during the Northern Hemispheric summer. Large phase errors (Fig. 8) have been found in the wind term (Fig. 8b) in comparison with the pressure (Fig. 8c) and total (Fig. 8a) terms.

3.3 Polar motion (wobble)

The displacement of the pole of rotation around the geographical reference pole, has been calculated according to equation (2.19). Before the discussion of the results, let us consider the first effect of a simple excitation function $\psi(Y_1, Y_2)$ to the wobble equation as defined by Barnes et al. (1983).

$$m + (i/\sigma_0)\dot{m} = \psi \tag{3.1}$$

If $\psi(Y_1, Y_2)$ is constant, then the solution is an anticlockwise motion of the pole of rotation around the excitation pole, with an angular velocity σ_0 and radius of $(m(0)-\psi)$. When ψ is a function of time, the pole of rotation follows a non-circular path. The component (Y_1, Y_2) are related to (X_1, X_2) by the expression

$$Y_1 = X_1 + \dot{X}_2/\Omega$$

$$Y_2 = X_2 - \dot{X}_1/\Omega \tag{3.2}$$

Global components Y_1, Y_2 have been calculated (figures are not shown). The Y_1, Y_2 follow the fluctuations of X_1, X_2 suggesting that the terms $\dot{X}_1/\Omega$ and $\dot{X}_2/\Omega$ are of smaller magnitude. Since $|\dot{m}/\sigma| \sim |m|$ (Barnes et al., 1983) the following relation has been adopted (derived from (2.19)) for calculating initial values of X_1, X_2

$$X_1 \sim m_1 - m_2$$

$$X_2 \sim m_1 + m_2 \tag{3.3}$$

If the initial coordinates (m_1^0, m_2^0) of the pole are known, then from (3.3) the initial values (X_1^0, X_2^0) can be estimated. The initial location of the geographical pole (m_1^0=0.1952, m_2^0=0.178 for 1986 and $m_1^0=9.6510^{-2}$, m_2^0=0.385 for 1987) has been chosen to have the position given by Bureau International de L'Heure (BIH) for the first of January 1986 and 1987 respectively.

The pole displacement calculated by equation (2.19) is strongly dependent on the position of the initial geographical pole. Below, an attempt will be made to investigate the pole movements, bearing

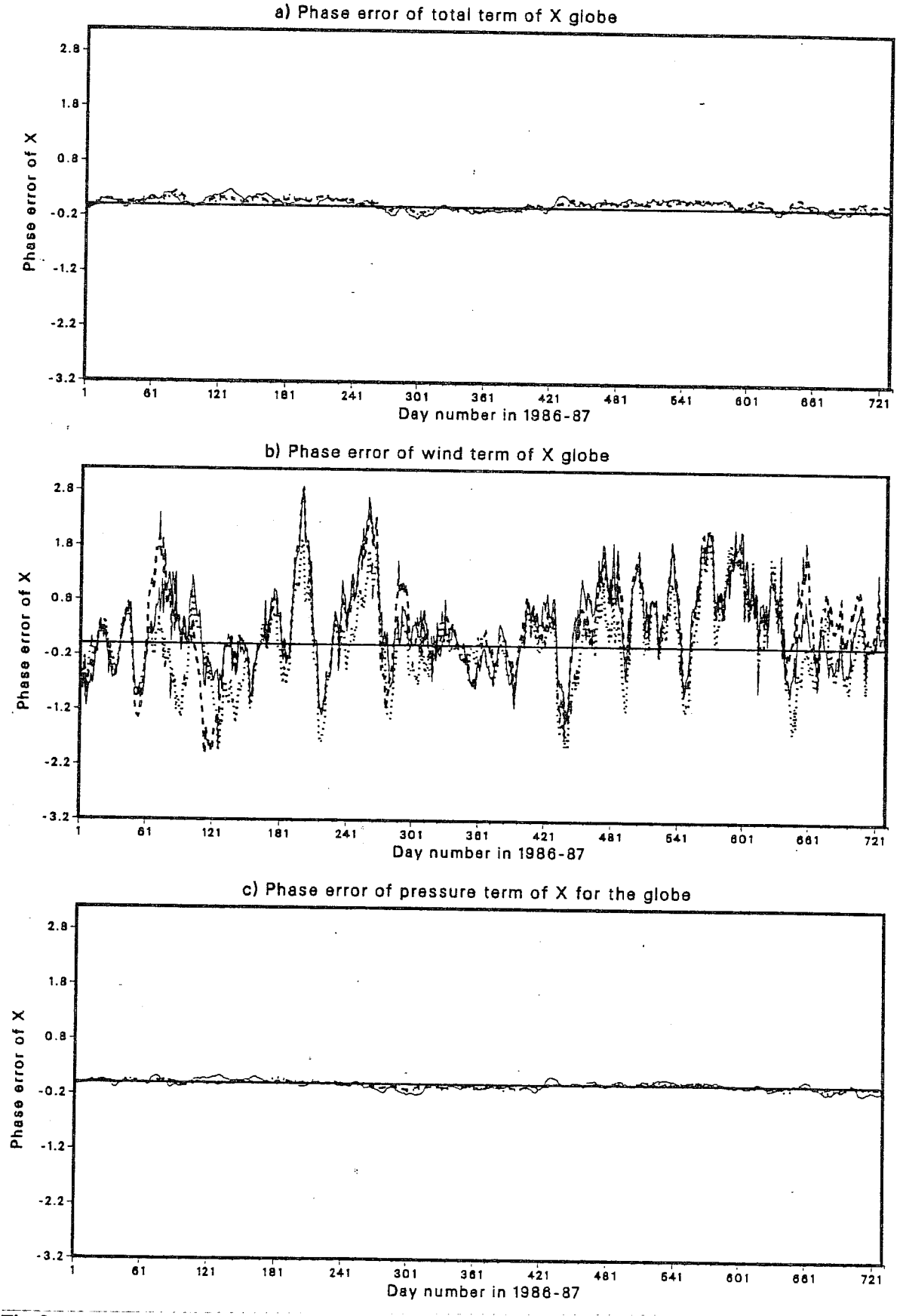

Fig. 8 As in Fig. 7 but for the prognostic phase error, which has been defined in Section 3.2. The phase error of the analysis is zero.

in mind that different results may be obtained if another position is chosen. The observed pole displacements can be considered as a result of surface loading, resulting from pressure and frictional stresses acting on the surface of the earth. Fluctuations in the equatorial components of AEAM functions play an important role in moving the earth's rotation pole (Barnes et al., 1983), and can even account for many of the detailed features of the observed polar motion. As was mentioned before, the pole's displacement around the geographical pole has been calculated from equation (2.19), using time series of the equatorial component of the AEAM functions X_1, X_2 for 1986 and 1987.

3.3.1 Northern Hemispheric contribution to the wobble

A comparison of Figs. 9e and 10e with 9a and 10a respectively reveals that the radius of the circle produced by the pressure term (X_1^p, X_2^p) is slightly larger than that produced by the total (X_1, X_2), suggesting that for both years, on average, the surface loading due to the wind term (X_1^w, X_2^w) is partly compensating the surface loading due to the pressure term (X_1^p, X_2^p). The wind term plays a minor role in pole displacement, since the radius of the circle forced by this term (Figs. 9c, 10c) is the smallest. The pole is moved anticlockwise by both terms, but the wind term moves the pole in an opposite direction to the pressure term, resulting in a smaller total (wind + pressure) radius.

For 1986 the radius of the circle forced by the wind term (Fig. 9c) is systematically smaller when calculated using forecast fields from the analyses. This means that the loading effects on the surface produced by changes in the prognostic wind term are lower than computed using analyses, and therefore there is a need for this torque to be increased. This torque appears to have been increased in the right direction by the introduction of gravity-wave drag in 1987 (Fig. 10c) but it seems that this increase was too much. For 1987 the 3-day radius of the prognostic cycle forced by the pressure term is systematically smaller than the analysed one. Therefore the pressure field has been slightly affected by gravity-wave drag as well, assuming natural interannual variability not to be the cause.

3.3.2 Southern Hemispheric contribution to the wobble

For the Southern Hemisphere the radius of the cycle produced by the total component (X_1, X_2) (Figs. 9b, 10b) is slightly greater than the one produced by pressure term (Figs. 9f, 10f). This suggests that, on average, the wind contribution to the wobble is of the same sign as the pressure contribution. The pole is moving anticlockwise by both contributions. Since the prognostic radius due to the wind term (Figs. 9d, 10d) is larger than the analysis and since by both terms the pole is moving in the same direction, the circle forced by the total term is of larger radius than the analyses values (Figs. 9b, 10b).

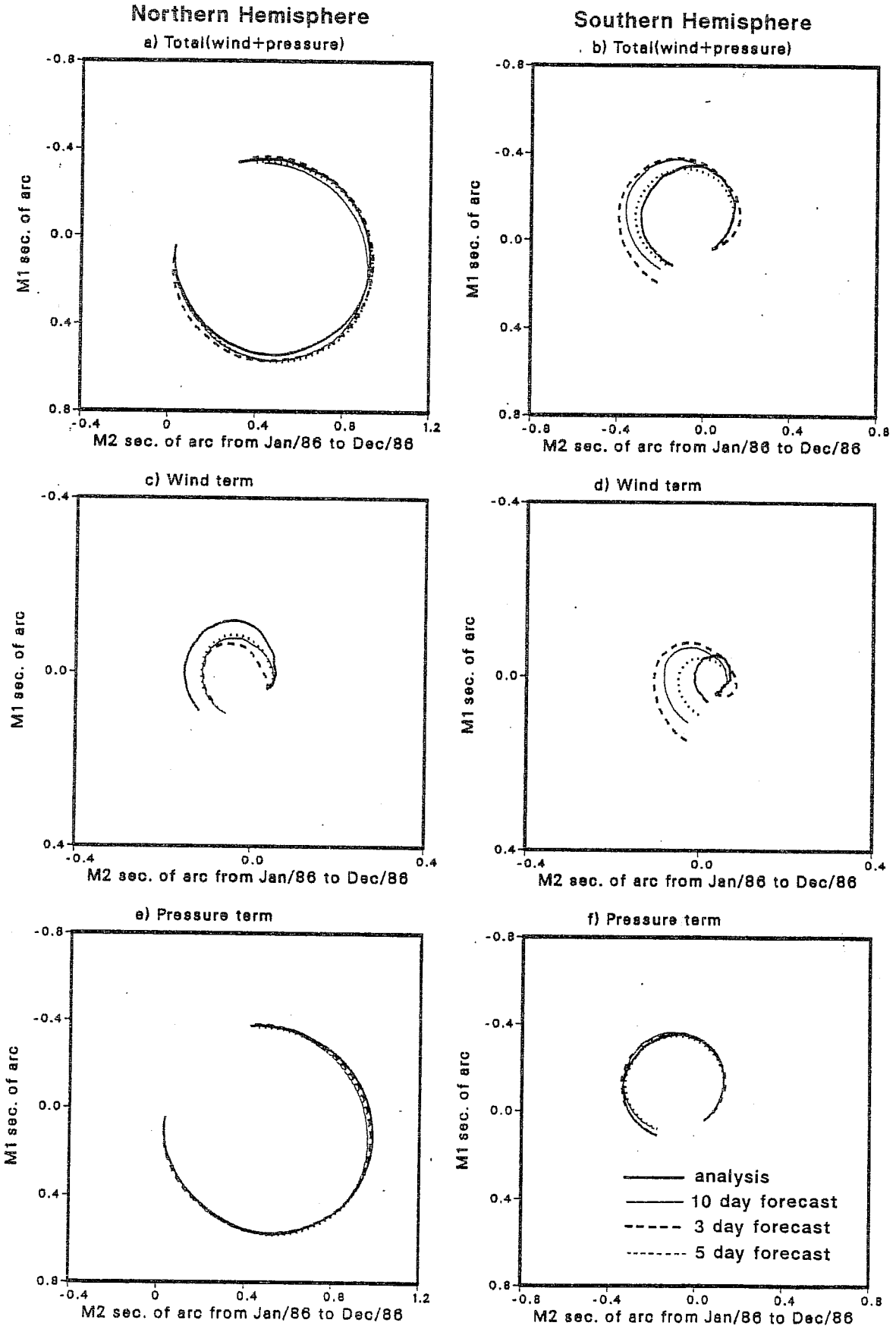

Fig. 9 Paths of the pole of rotation around the geographical reference pole for the Northern and Southern Hemispheres for 1986. The convention for the type of curve is the same as in Fig. 1.

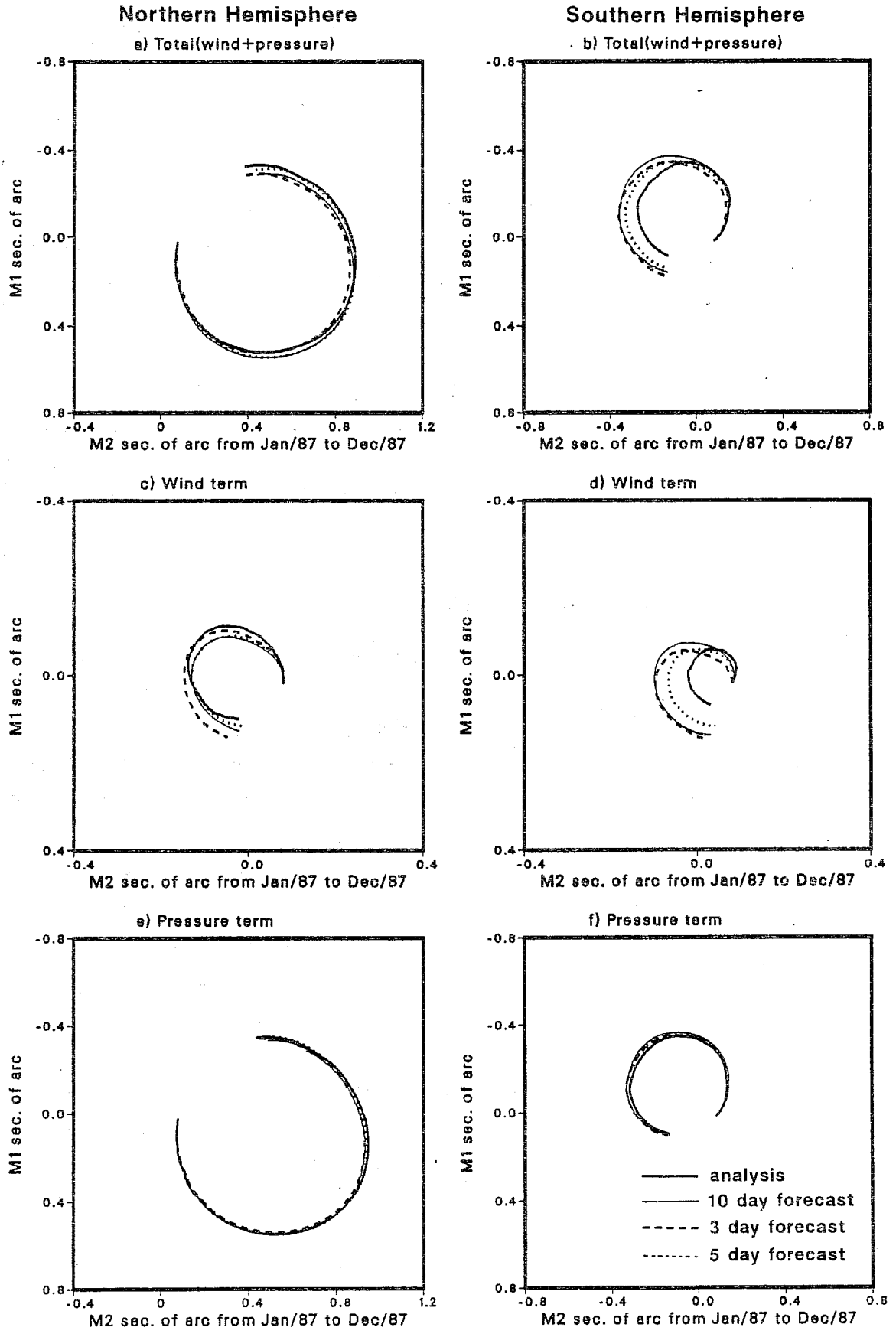

Fig. 10 As in Fig. 9 but for 1987.

There is a systematic error in the wind term in the Southern Hemisphere (Figs. 9d, 10d) and the radius of the prognostic circles are larger than those of the analyses. Therefore the torque produced by the wind term in the Southern Hemisphere is larger than the one produced by the analysis, and there is a need for this torque to be decreased.

Another systematic error appears in the pressure term for 1987. The radius of the predicted cycle is higher than that of the analyses, suggesting that the surface loading produced by the pressure term should be reduced. There is evidence of the spin-up problem, since the largest radius is found in the 3-day prognostic circle forced by the (X_1^W, X_2^W).

3.4 Axial component of atmospheric effective angular momentum functions

While the redistribution of air mass is mainly responsible for altering the equatorial component of the AEAM function, the strengthening or weakening of the zonal winds (as described by the second term of the equation 2.23) is predominantly responsible for changing the axial component of the AEAM function.

3.4.1 Northern Hemispheric contribution to X_3

The terms X_3^W calculated from initialized analyses and forecasts for both years (Fig. 11b) show the familiar annual pattern (see for example, Rosen and Salstein, 1983; Barnes et al., 1983). Due to strong westerlies during the winter there is a maximum at the end of January, which begins to decrease late in February, followed by a steady fall until it becomes negative around July. It then rises again returning to a maximum by late January. A study of X_3^W (Fig. 11b) reveals that since the middle of 1986 there has been an error in the forecast, with the prognostic values of X_3^W systematically underestimated in comparison to those of the initialized analyses. This systematic error continues to exist during 1987 and may be related to the introduction of parametrized gravity-wave drag, since the time of occurrence coincides with the introduction of this process in the model. The systematic error of the model's atmosphere is such that it loses angular momentum, associated with a weakening and northward shift of mid-latitude westerly flow, or increase in tropical easterlies. Either the gravity-wave drag is higher than the optimum one, or its introduction has revealed the presence of what was formerly a compensating error. Since the pressure term X_3^p makes a minor contribution to fluctuations in atmospheric axial effective angular momentum the quantity, X_3^p - mean (X_3^p) has been plotted in Fig. 11c. The mean of X_3^p has been determined for the period 1986-1987. It is not clear if there is any systematic error. There is an annual variation with rapid variations superimposed. The total variation of X_3 - mean (X_3), is shown in Fig. 11a. The annual variation of the total is similar to that of the wind term.

3.4.2 The Southern Hemispheric contribution to X_3

As in the Northern Hemisphere there is a minimum in the axial X_3^W component (Fig. 12b) during the Southern Hemispheric summer owing to a weakening of the zonal winds (late February); the curve then

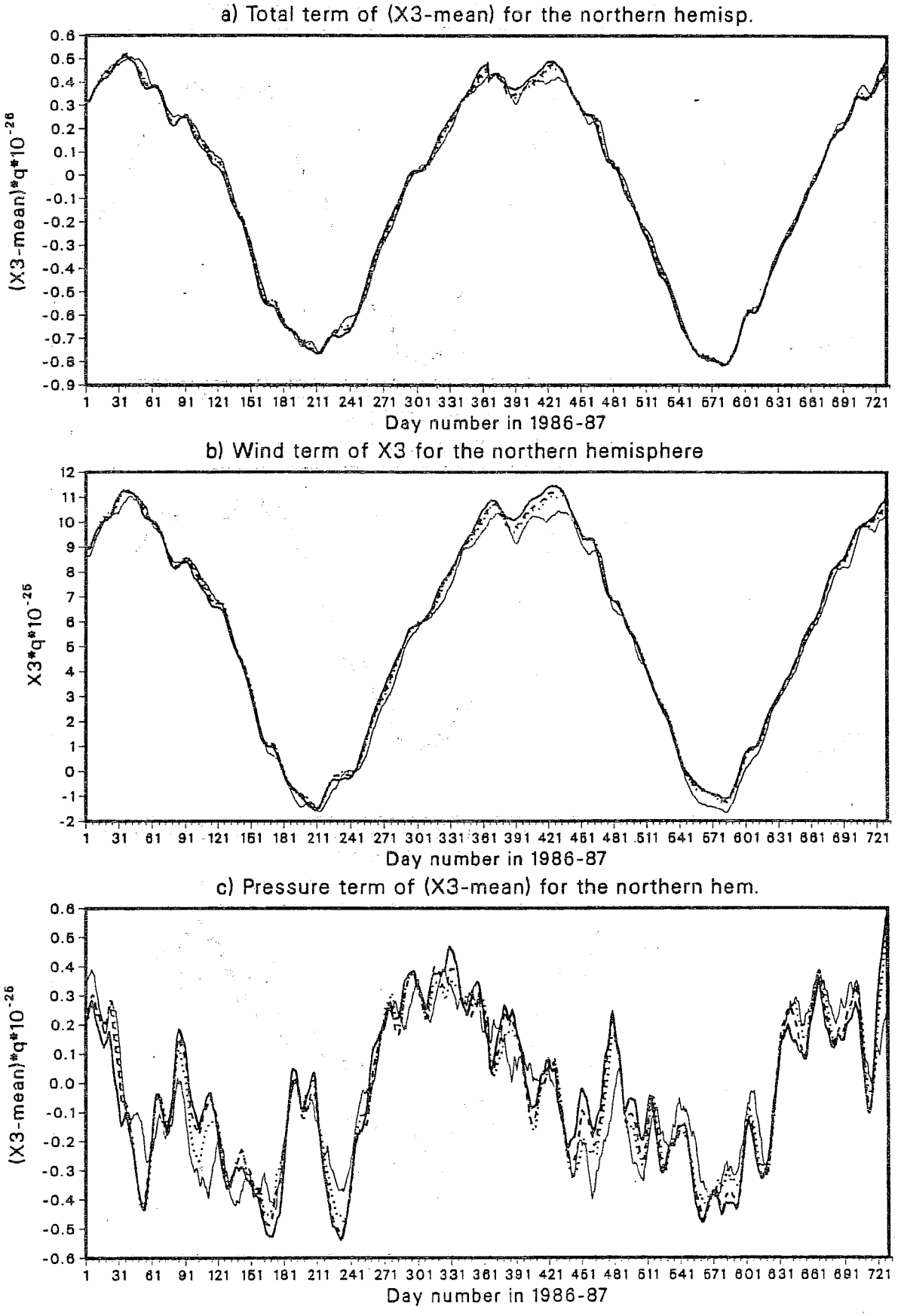

Fig. 11 As in Fig. 1 but for the axial component of X_3.

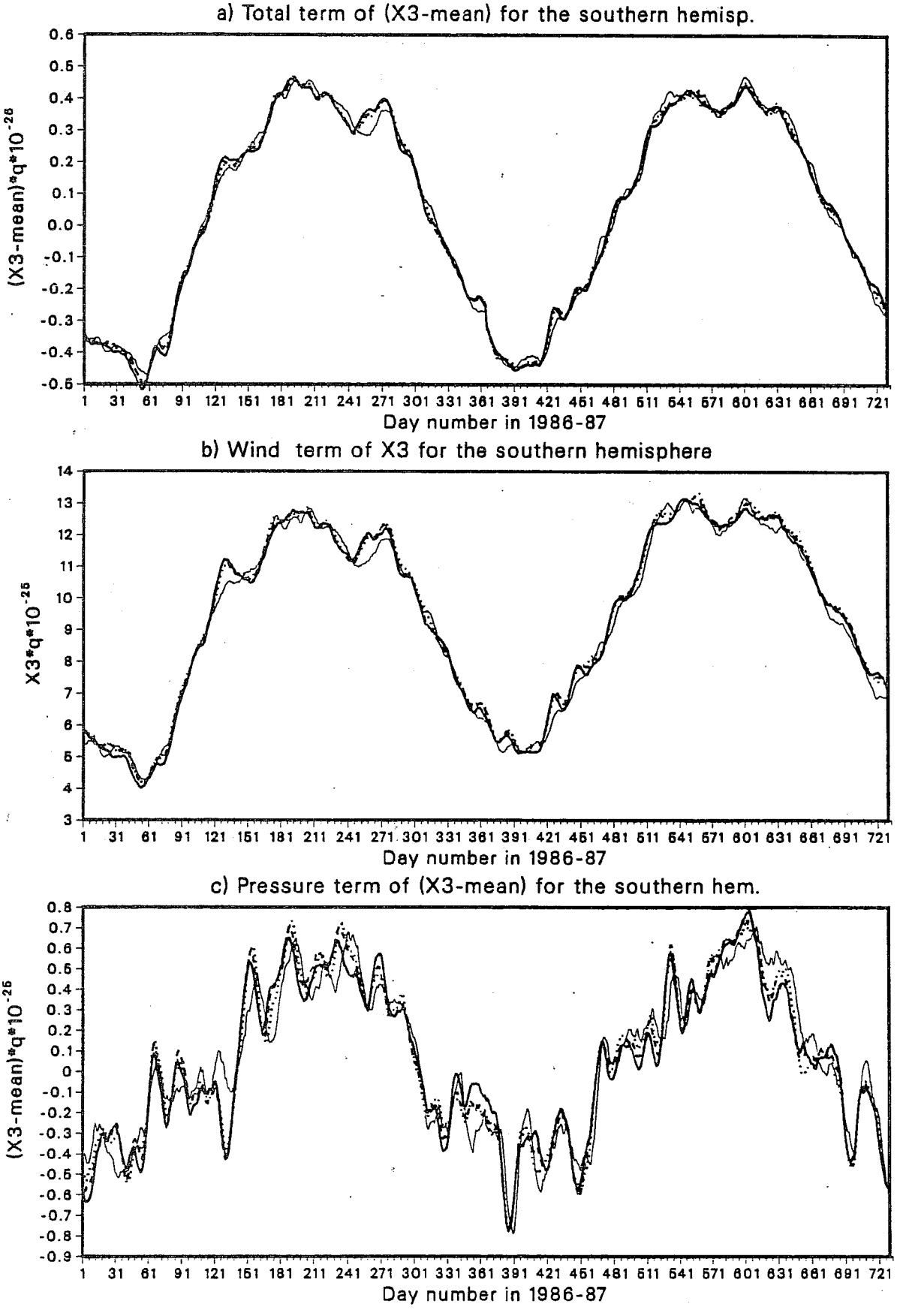

Fig. 12 As in Fig. 11 but for the Southern Hemisphere.

rises steadily up to end of May, remains at the same level up to the end of the winter and then fallsuntil it again reaches a minimum by February. The maximum of X_3^W occurs during the Southern Hemispheric winter, when the rotation of the atmosphere relative to the earth is at maximum, due to strong westerlies. The Southern Hemispheric maxima and minima are 180 degrees out of phase with those of the Northern Hemisphere. In contrast to the Northern Hemisphere there is no significant systematic error, which, in view of inter-hemispheric differences in the distribution of orography is consistent with the suggestion that the Northern Hemispheric systematic error is related to the introduction of gravity-wave drag.

There is an annual variation of X_3^p - mean (X_3^p) (Fig. 12a) similar to X_3^W with more small variations superimposed. The curve of total X_3- mean (X_3) (Fig. 12a) follows the variation of X_3^W as well.

3.4.3 The global contribution to X_3

In the global curves (Fig. 13), the characteristics of the Northern Hemisphere are dominant, since the amplitude of annual variations of X_3 are higher in the Northern Hemisphere. There is a maximum of X_3^W (Figs. 13b) during the Northern Hemispheric winter and a minimum in the Northern Hemispheric summer. Since the angular momentum about the X_3-axis in the Earth-Atmosphere system is conserved, there should be an exchange of angular momentum between the Earth and the atmosphere, as we will see later. In 1986 there is a secondary maximum in X_3^W during September besides the main maximum in May. The curve falls steadily and remains low during summer (up to end of August) and then rises steadily up to its maximum value. For 1987 the secondary maximum is in January, followed by a main maximum in March. Superimposed on the annual variation is a low frequency variability with a period of about 30 days in the pressure term.

From the middle of 1986 onwards, there is a considerable error in the 10 day forecast, and the model's atmosphere is losing axial angular momentum. The fluctuations in the pressure term (Figs. 11c) show major maxima of fluctuations in the 10-day forecast. Finally there is a weak minimum within the Northern Hemispheric summer in the total axial angular momentum (Fig. 13a).

3.5 Changes in the length-of-day

Using monthly mean zonal wind data, Lambeck and Cazenave (1974) concluded that all irregular variations in the earth's rotational frequencies between 0.3 and 0.6 cycle per year are of meteorological origin. Hide et al. (1980) showed that even short-term changes in length-of-day are well correlated with fluctuations in the axial angular momentum of the atmosphere. Langley et al. (1981) have found good agreement of short time-scales changes with length-of-day. Barnes et al. (1983) showed that during most of the period from 1 January 1981 to 30 April 1982 there is a good agreement between meteorological and astronomical curves, suggesting that short-term changes in the length-of-day are due to angular momentum exchange between the atmosphere and the solid earth.

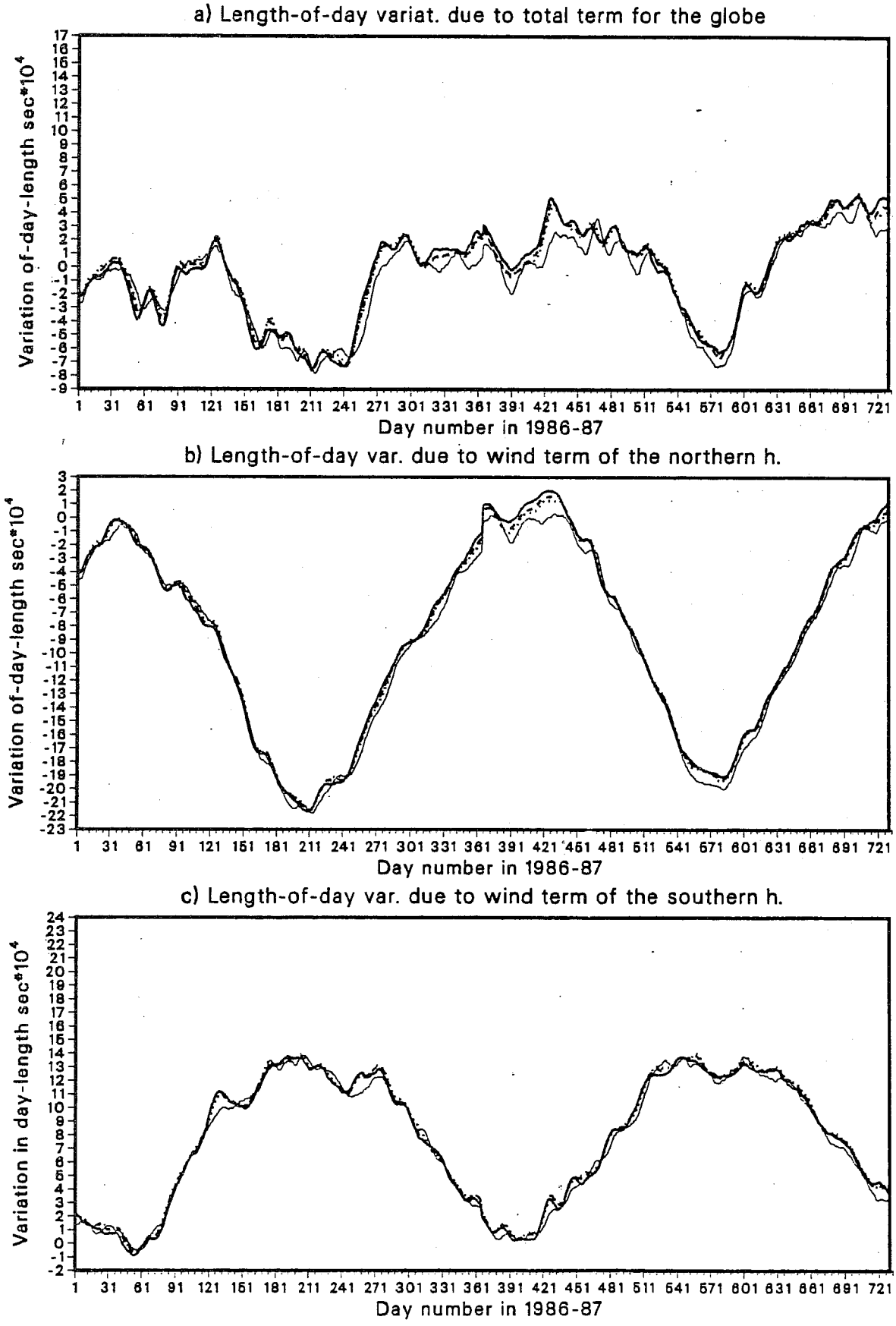

Fig. 13 As in Fig. 11 but for the Globe.

For our studies, changes in length-of-day have been estimated by equation (2.11).

$$\Lambda = \frac{2\pi}{\omega_3}$$

where Λ is the length-of-day, $\omega_3 = (1+m_3)\,\Omega$ and $m_3 = Y_3 + c$. Estimation of Λ requires the evaluation of the integration constant c, which in this study has been chosen to produce a length-of-day exactly equal to $2\pi/\Omega$ at the beginning of the year (1 January for 1986 and 1987).

3.5.1 Northern Hemispheric contribution to length-of-day variations

Since changes in the distribution and strength of zonal wind provide the main contribution to fluctuations in X_3, the wind contribution to the length-of-day is shown in Fig. 14b. For both years, there is a maximum in length-of-day during late winter (late February or beginning of March) showing that the solid earth is rotating slowly, then the curves fall steadily until they reach their minimum in early July (meaning that the earth is rotating faster), and they then rise steadily up to a maximum value. There is an error which is similar to the Northern Hemispheric systematic error of X_3^W, and the model's length-of-day is shorter than that of the analyses, corresponding to an increase of angular momentum of the solid earth.

3.5.2 Southern Hemispheric contribution to length-of-day variations

The Southern Hemispheric variations in the length-of-day (Fig. 14c) are the same as those of the Northern Hemisphere in the sense that both maxima occur during each hemisphere's winter and the minima during the summers. The curve of the length-of-day for the Southern Hemisphere is 180 degrees out of phase with the Northern one. Due to more orography and land-sea contrast in the Northern Hemisphere the amplitude of the length-of-day curve is about 35% larger than of the Southern Hemisphere curve. The error apparently induced in the Northern Hemisphere by the parametrization of the gravity-wave drag cannot be traced in the Southern Hemisphere.

3.5.3 Global contribution to length-of-day variations

Due to the fact that the length-of-day amplitude is higher in the Northern Hemisphere, the characteristics of the Northern Hemisphere are dominant in the global length-of-day curves (Fig. 14a). For both years the maximum occurs during the Northern Hemispheric winter and the minimum during the Northern Hemispheric summer.

4. CONCLUSIONS

Time series of wind and surface pressure have been used to evaluate AEAM functions, polar motion and length-of-day for 1200 GMT initialized analyses, and 3-, 5- and 10-day forecasts, using archived

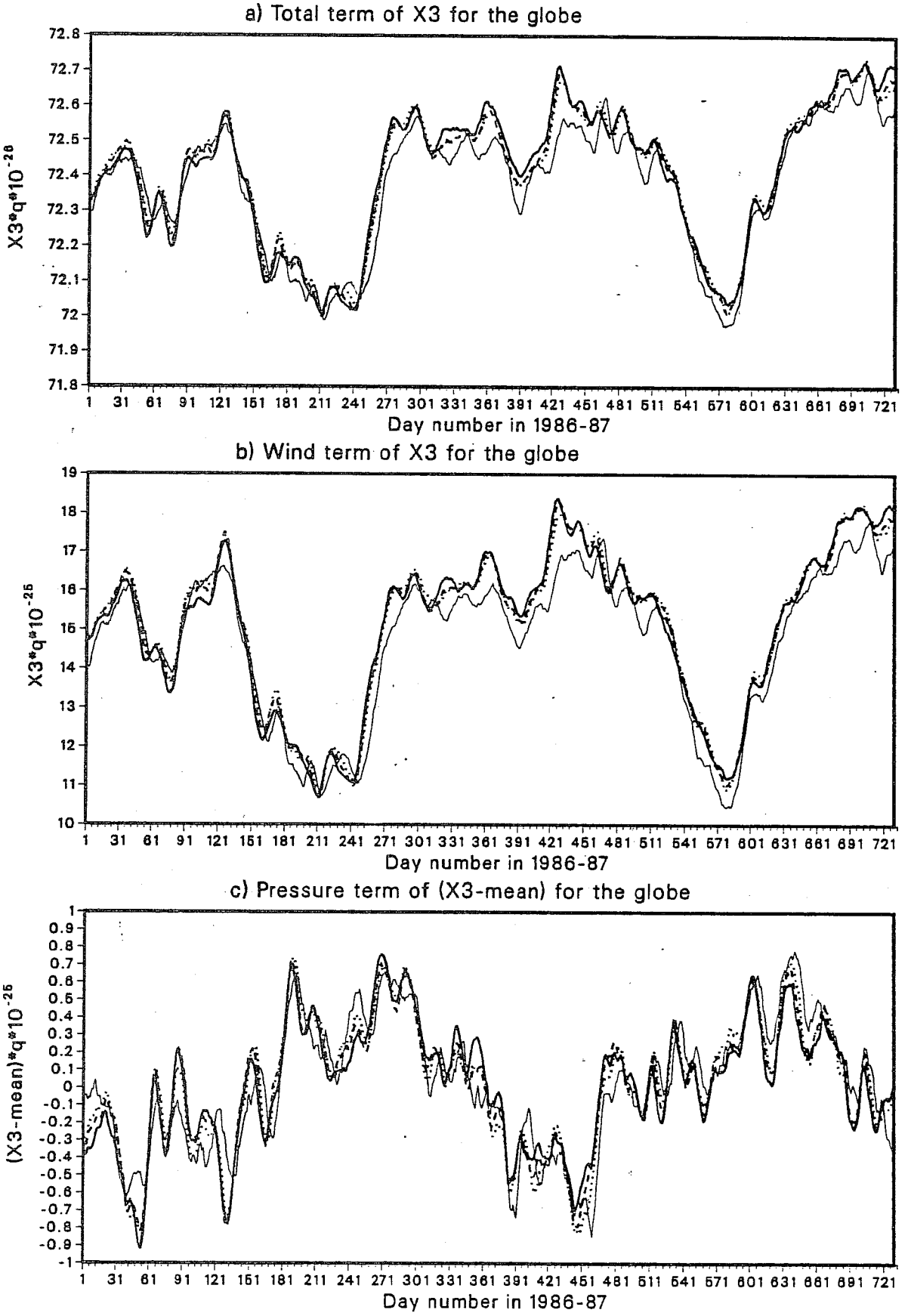

Fig. 14 Variation in length-of-day for the Globe, Northern and Southern Hemisphere for 1986-1987. The convention for the type of curve is the same as in Fig. 1.

ECMWF data. The conclusions will be discussed separately for the equatorial component, polar motion and axial component.

4.1 Equatorial AEAM function (X_1, X_2)

In the Northern Hemisphere the term X_2^p is of higher order than X_1^p and exhibits a marked annual variation, which is opposite to X_2^w. Therefore the amplitude of the total X_2 is smaller than X_2^p. The yearly variation of X_1^w is opposite to X_1^p as well and the amplitude of X_1^p is smaller than X_2^p.

In the Southern Hemisphere the amplitudes of the annual variations of X_1^w, X_2^w, X_1^p and X_2^p are very small. This shows the dependence of X_1 and X_2 on orography and land-sea contrast. Globally, on average the wind terms X_1^w and X_2^w are working in an opposite direction to yearly variations of X_1^p and X_2^p, respectively.

The main systematic error is connected to the wind terms, and the model atmosphere's tendency is to overestimate X_1^w and X_1^p in the Northern and underestimate X_2^w in the Southern Hemisphere. A large error in the wind term of X_2 in the Southern Hemisphere is found to be related to the wind error. An analysis of the phase error of $X=X_1+iX_2$ shows the existence of a large error in the wind term.

4.2 Polar motion

Due to redistribution of mass (measured for example by changes in surface pressure) there are loading effects on the earth surface. The loading on the earth's surface (produced by the Northern Hemisphere pressure term) forces the pole of rotation to move anticlockwise around the geographical pole. On average, it has been found that the wind terms (in both Hemispheres) and the Southern Hemispheric pressure term move the rotation pole anticlockwise, but the motion is 180 degrees out of phase with respect to that produced by the Northern Hemispheric pressure term. This explains why the radius of the resultant motion (total term) is smaller than that produced by the Northern Hemispheric pressure term. With respect to the systematic error in implied polar movements, the following has been found. For 1986 the radius of the circle produced by the predicted Northern Hemisphere wind term is systematically smaller than the one forced by the wind term of the initialized analysis. This indicates that the prognostic torque is smaller than that produced by the initialized analysis. This torque has been increased by the introduction of gravity-wave drag for 1987, and the sign of the error reversed, indicating that either the drag is higher than required or there is another error source which is no longer compensated by a lack of parametrized wave-drag.

For the Southern Hemisphere the radius of the prognostic circle (forced by the wind term) is much higher than that of the initialized analyses. Therefore there is too much torque in the model

atmosphere of the Southern Hemisphere. A systematic error appears in the pressure term as well after the introduction of the parametrization of gravity-wave drag.

4.3 Axial AEAM function

In accordance with previous studies it is found that the variation in X_3 is mainly due to wind variations. Looking into the annual variation of X_3^W (Fig. 11b) in connection with length-of-day variations (Fig. 14b) it can be seen that there is an exchange of angular momentum between the atmosphere and the earth. During the Northern Hemispheric winter the X_3^W is at maximum (due to strong westerlies) and the length-of-day curve has its maximum, with an implied transfer of angular momentum from the solid earth to the atmosphere. During the Northern Hemispheric summer there is a minimum in X_3^W (due to a weakening and northward shift of the westerlies) and a minimum in length-of-day, resulting in a transfer of angular momentum from the atmosphere to the solid earth. The same happens in the Southern Hemisphere (Figs. 12b, 14c), during the Southern Hemispheric winter where besides the inter-hemispheric transfer within the atmosphere, there is a transfer of angular momentum from the solid earth to the atmosphere and vice versa during summer. Due to the phase difference between the seasons in both Hemispheres, the resultant net transfer is small.

Comparison of the predicted X_3^W with that calculated from the initialized analyses shows that a systematic error has been introduced in the model following the incorporation of gravity-wave drag. Since the middle of 1986 (Fig. 11b) the prognostic X_3^W are systematically smaller than those estimated from the initialized analyses. This indicates that the model's atmospheric angular momentum is smaller than that of the initialized analyses. From Fig. 14b there is a corresponding systematic error as well in length-of-day, and the models implied length-of-day is shorter than that of the analysis resulting in a higher rate of transfer of angular momentum from the atmosphere to the earth.

Finally, considering the main modelling implications to the effective angular momentum functions, it may be concluded that:

1) The systematic error in the Northern Hemisphere X_3^W term, apparently introduced by the incorporation of gravity-wave drag into the model, is probably due to a compensating error. Preliminary first results show that the northward shift of mid-latitude westerly flow has been reduced, after the incorporation of the new vertical diffusion into the model. This systematic error could be a consequence of the use of both gravity-wave drag and the envelope orography.

ii) The large biases in the X_2 wind term of the Southern Hemisphere arises from the large wind error in this hemisphere, the causes of which are not well understood.

References

Barnes, R.T.H., R. Hide, A.A. White and C.A. Wilson, 1983: Atmospheric angular momentum fluctuations, length-of-day changes and polar motion. Proc. R. Soc. Lond., A, 387, 31-73.

Chandler, S., 1891a: On the variation of latitude. Astronomical 11, 83.

Chandler, 1891b: On the supposed secular variation of latitude. Astronomical 11, 109.

Chandler, S., 1892: On the variation in latitude. Astronomical 12, 17.

Hide, R., N.T. Birch, L.V. Morrison, D.J. Shea and A.A. White., 1980: Atmospheric angular momentum fluctuations and changes in the length of the day. Nature, 286, 114-117.

Illari, L., 1987: The "spin-up" problem. Tech. Memo. No. 137, ECMWF, 30 pp.

Lambeck, K. and A. Cazenave, 1974: The Earth's rotation and atmospheric circulation - II. The continum Geophys., J.R. Astr. Soc., 38, 49-61.

Lambeck, K., 1980: The earth's variable rotation: geophysical causes and consequences. Cambridge University Press, 449 pp.

Langley, R.B., R.W. King, I.I. Shapiro, R.D. Rosen and D.A. Salstein, 1981: Atmospheric angular momentum and length of day: a common fluctuation with period near 50 days. Nature, 294, 730-732.

Miller, M.J. and T.N. Palmer, 1987: Orographic gravity-wave drag: Its parametrization and influence in general circulation and numerical weather prediction models. ECMWF Seminar/workshop on Observation, Theory and Modelling of Orographic Effects, 15-20 September 1986, Vol. 1, 283-333.

Munk, W.H. and G.J.F. MacDonald, 1960: The rotation of the earth. Cambridge University Press, 393 pp.

Rosen, R.D. and D.A. Salstein, 1983: Variations in atmospheric angular momentum on global and regional scales and the length of day. J.Geophys.Res. 88, 5451-5470.

Routh, E., 1905: Dynamics of a system of rigid bodies. Part II. New York: MacMillan. Republished by Dover Publications 1955.

Shaw, D.B., P. Lönnberg, A. Hollingsworth and P. Undén, 1987: Data assimilation: The 1984/85 revisions of the ECMWF mass and wind analysis. Quart.J.R.Met.Soc., 113, 533-566.

Simmons, A.J., D.M. Burridge, M. Jarraud, C. Girard and W. Wergen, 1988: The ECMWF medium range prediction models, development of the numerical formulations and the impact of increased resolution. Met. + Atmos. Phys. To be published.

Tiedtke, M., W. Heckley and J. Slingo, 1988: Tropical forecasting at ECMWF: The influence of physical parametrization on the mean structure of forecasts and analysis. Quart.J.Roy.Met.Soc., 114, 639-664.

Tiedtke, M., J.-F. Geleyn, A. Hollingsworth and J.-F. Louis, 1979: ECMWF model parametrization of sub-grid scale processes. ECMWF Tech. Rep. No. 10, 46 pp.

TECHNICAL REPORTS

No. 1 A case study of a ten day prediction.
K. Arpe, L. Bengtsson, A. Hollingsworth and Z. Janjic. September, 1976

No. 2 The effect of arithmetic precision on some meteorological integrations.
A.P.M. Baede, D. Dent and A. Hollingsworth. December, 1976

No. 3 Mixed-radix fourier transforms without reordering.
C. Temperton. February, 1977

No. 4 A model for medium range weather forecasts - adiabatic formulation.
D.M. Burridge and J. Haseler. March, 1977

No. 5 A study of some parameterisations of sub-grid processes in a baroclinic wave in a two dimensional model.
A. Hollingsworth. July, 1977

No. 6 The ECMWF analysis and data assimilation scheme: analysis of mass and wind field.
A. Lorenc, I. Rutherford and G. Larsen. December, 1977

No. 7 A ten-day high-resolution non-adiabatic spectral integration; a comparative study.
A.P.M. Baede and A.W. Hansen. October, 1977

No. 8 On the asymptotic behaviour of simple stochastic-dynamic systems.
A. Wiin-Nielsen. November, 1977

No. 9 On balance requirements as initial conditions.
A. Wiin-Nielsen. October, 1978

No. 10 ECMWF model parameterisation of sub-grid scale processes.
M. Tiedtke, J-F. Geleyn, A. Hollingsworth, and J-F. Louis. January, 1979

No. 11 Normal mode initialization for a multi-level grid-point model.
C. Temperton and D.L. Williamson. April, 1979

No. 12 Data assimilation experiments.
R. Seaman. October, 1978

No. 13 Comparison of medium range forecasts made with two parameterisation schemes.
A. Hollingsworth, K. Arpe, M. Tiedkte, M. Capaldo, H. Savijarvi, O. Akesson and J.A. Woods. October, 1978

No. 14 On initial conditions for non-hydrostatic models.
A.C. Wiin-Nielsen. November, 1978

No. 15 Adiabatic formulation and organization of ECMWF's spectral model.
A.P.M. Baede, M. Jarraud and U. Cubasch. November, 1979

No. 16 Model studies of a developing boundary layer over the ocean.
H. Okland. November, 1979

No. 17 The response of a global barotropic model to forcing by large scale orography.
J. Quiby. January 1980.

No. 18 Confidence limits for verification and energetic studies.
K. Arpe. May, 1980

No. 19 A low order barotropic model on the sphere with orographic and newtonian forcing.
E. Kallen. July, 1980

No. 20 A review of the normal mode initialization method.
Du Xing-yuan. August, 1980

No. 21 The adjoint equation technique applied to meteorological problems.
G. Kontarev. September, 1980

No. 22 The use of empirical methods for mesoscale pressure forecasts.
P. Bergthorsson. November, 1980

No. 23 Comparison of medium range weather forecasts made with models using spectral or finite difference techniques in the horizontal.
M. Jarraud, C. Girard and U. Cubasch. February, 1981

No. 24 On the average error of an ensemble of forecasts.
J. Derome. February, 1981

No. 25 On the atmospheric factors affecting the Levantine Sea.
E. Ozsoy. May, 1981

No. 26 Tropical influences on stationary wave motion in middle and high latitudes.
A.J. Simmons. August, 1981

No. 27 The energy budgets in North America, North Atlantic and Europe based on ECMWF analysis and forecasts.
H. Savijarvi. November, 1981

No. 28 An energy and angular momentum conserving finite-difference scheme, hybrid coordinates and medium range weather forecasts.
A.J. Simmons and R. Strüfing. November, 1981

No. 29 Orographic influences on Mediterranean lee cyclogenesis and European blocking in a global numerical model.
S. Tibaldi and A. Buzzi. February, 1982

No. 30 Review and re-assessment of ECNET - A private network with open architecture.
A. Haag, F. Konigshofer and P. Quoilin. May, 1982

No. 31 An investigation of the impact at middle and high latitudes of tropical forecast errors.
J. Haseler. August, 1982

No. 32 Short and medium range forecast differences between a spectral and grid point model. An extensive quasi-operational comparison. C. Girard and M. Jarraud
August, 1982

No. 33 Numerical simulations of a case of blocking: The effects of orography and land-sea contrast.
L.R. Ji and S. Tibaldi. September, 1982

No. 34 The impact of cloud track wind data on global analyses and medium range forecasts.
P. Kallberg, S. Uppala, N. Gustafsson and J. Pailleux. December, 1982

No. 35 Energy budget calculations at ECMWF. Part 1: Analyses 1980-81.
E. Oriol. December, 1982

No. 36 Operational verification of ECMWF forecast fields and results for 1980-1981.
R. Nieminen. February, 1983

No. 37 High resolution experiments with the ECMWF model: a case study.
L. Dell'Osso. September, 1983

No. 38 The response of the ECMWF global model to the El-Nino anomaly in extended range prediction experiments.
U. Cubasch. September, 1983

No. 39 On the parameterisation of vertical diffusion in large-scale atmospheric models.
M.J. Manton. December, 1983

No. 40 Spectral characteristics of the ECMWF objective analysis system.
R. Daley. December, 1983

No. 41 Systematic errors in the baroclinic waves of the ECMWF model.
E. Klinker and M. Capaldo. February, 1984

No. 42 On long stationary and transient atmospheric waves.
A.C. Wiin-Nielsen. August, 1984

No. 43 A new convective adjustment scheme.
A.K. Betts and M.J. Miller. October, 1984

No. 44 Numerical experiments on the simulation of the 1979 Asian summer monsoon.
U.C. Mohanty, R.P. Pearce and M. Tiedtke. October, 1984

No. 46 Cloud prediction in the ECMWF model.
J. Slingo and B. Ritter. January, 1985

No. 47 Impact of aircraft wind data on ECMWF analyses and forecasts during the FGGE period, 8-19 November, 1979.
A.P.M. Baede, P. Kallberg and S. Uppala. March, 1985

No. 48 A numerical case study of East Asian coastal cyclogenesis.
Shou-jun Chen and L. Dell'Osso. May, 1985

No. 49 A study of the predictability of the ECMWF operational forecast model in the tropics.
M. Kanamitsu. September, 1985

No. 50 On the development of orographic cyclones.
D. Radinovic. June, 1985

No. 51 Climatology and system error of rainfall forecasts at ECMWF.
F. Molteni and S. Tibaldi. October, 1985

No. 52 Impact of modified physical processes on the tropical simulation in the ECMWF model.
U.C. Mohanty, J.M. Slingo and M. Tiedtke. October, 1985

No. 53 The performance and systematic errors of the ECMWF tropical forecasts (1982-1984).
W.A. Heckley. November, 1985

No. 54 Finite element schemes for the vertical discretization of the ECMWF forecast model using linear elements.
D.M. Burridge, J. Steppeler and R. Strüfing. January, 1986

No. 55 Finite element schemes for the vertical discretization of the ECMWF forecast model using quadratic and cubic elements.
J. Steppeler. February, 1986

No. 56 Sensitivity of medium-range weather forecasts to the use of an envelope orography.
M. Jarraud, A.J. Simmons and M. Kanamitsu. September, 1986

No. 57 Zonal diagnostics of the ECMWF 1984-85 operational analyses and forecasts.
C. Brankovic. October, 1986

No. 58 An evaluation of the performance of the ECMWF operational forecasting system in analysing and forecasting tropical easterly wave disturbances. Part 1: Synoptic investigation.
R.J. Reed, A. Hollingsworth, W.A. Heckley and F. Delsol. September, 1986

No. 59 Diabatic nonlinear normal mode initialisation for a spectral model with a hybrid vertical coordinate.
W. Wergen. January, 1987

No. 60 An evaluation of the performance of the ECMWF operational forecasting system in analysing and forecasting tropical easterly wave disturbances. Part 2: Spectral investigation.
R.J. Reed, E. Klinker and A. Hollingsworth. January, 1987

No. 61 Empirical orthogonal function analysis in the zonal and eddy components of 500 mb height fields in the Northern extratropics.
F. Molteni. January, 1987